JCI The Journal of Clinical Investigation

Canonical WNT signaling components in vascular development and barrier formation

Yulian Zhou, … , Makoto M. Taketo, Jeremy Nathans

J Clin Invest. 2014;124(9):3825-3846. https://doi.org/10.1172/JCI76431.

Research Article **Vascular biology**

Canonical WNT signaling is required for proper vascularization of the CNS during embryonic development. Here, we used mice with targeted mutations in genes encoding canonical WNT pathway members to evaluate the exact contribution of these components in CNS vascular development and in specification of the blood-brain barrier (BBB) and blood-retina barrier (BRB). We determined that vasculature in various CNS regions is differentially sensitive to perturbations in canonical WNT signaling. The closely related WNT signaling coreceptors LDL receptor–related protein 5 (LRP5) and LRP6 had redundant functions in brain vascular development and barrier maintenance; however, loss of LRP5 alone dramatically altered development of the retinal vasculature. The BBB in the cerebellum and pons/interpeduncular nuclei was highly sensitive to decrements in canonical WNT signaling, and WNT signaling was required to maintain plasticity of barrier properties in mature CNS vasculature. Brain and retinal vascular defects resulting from ablation of Norrin/Frizzled4 signaling were ameliorated by stabilizing β-catenin, while inhibition of β-catenin–dependent transcription recapitulated the vascular development and barrier defects associated with loss of receptor, coreceptor, or ligand, indicating that Norrin/Frizzled4 signaling acts predominantly through β-catenin–dependent transcriptional regulation. Together, these data strongly support a model in which identical or nearly identical canonical WNT signaling mechanisms mediate neural tube and retinal vascularization and maintain the BBB and BRB.

Canonical WNT signaling components in vascular development and barrier formation

Yulian Zhou,[1] Yanshu Wang,[1,2] Max Tischfield,[1] John Williams,[1,2] Philip M. Smallwood,[1,2] Amir Rattner,[1] Makoto M. Taketo,[3] and Jeremy Nathans[1,2,4,5]

[1]Department of Molecular Biology and Genetics and [2]Howard Hughes Medical Institute, Johns Hopkins University School of Medicine, Baltimore, Maryland, USA. [3]Department of Pharmacology, Graduate School of Medicine, Kyoto University, Yoshida-Konoé-cho, Sakyo, Kyoto, Japan. [4]Department of Neuroscience and [5]Department of Ophthalmology, Johns Hopkins University School of Medicine, Baltimore, Maryland, USA.

Canonical WNT signaling is required for proper vascularization of the CNS during embryonic development. Here, we used mice with targeted mutations in genes encoding canonical WNT pathway members to evaluate the exact contribution of these components in CNS vascular development and in specification of the blood-brain barrier (BBB) and blood-retina barrier (BRB). We determined that vasculature in various CNS regions is differentially sensitive to perturbations in canonical WNT signaling. The closely related WNT signaling coreceptors LDL receptor–related protein 5 (LRP5) and LRP6 had redundant functions in brain vascular development and barrier maintenance; however, loss of LRP5 alone dramatically altered development of the retinal vasculature. The BBB in the cerebellum and pons/interpeduncular nuclei was highly sensitive to decrements in canonical WNT signaling, and WNT signaling was required to maintain plasticity of barrier properties in mature CNS vasculature. Brain and retinal vascular defects resulting from ablation of Norrin/Frizzled4 signaling were ameliorated by stabilizing β-catenin, while inhibition of β-catenin–dependent transcription recapitulated the vascular development and barrier defects associated with loss of receptor, coreceptor, or ligand, indicating that Norrin/Frizzled4 signaling acts predominantly through β-catenin–dependent transcriptional regulation. Together, these data strongly support a model in which identical or nearly identical canonical WNT signaling mechanisms mediate neural tube and retinal vascularization and maintain the BBB and BRB.

Introduction

In vertebrates, vascular endothelial cells (ECs) exhibit characteristic structural and functional differences among tissues (1, 2). For example, in renal glomeruli, numerous fenestrations pack the surfaces of capillary ECs, an arrangement that maximizes serum filtration (3). In contrast, in regions of the CNS with a blood-brain barrier (BBB) or blood-retina barrier (BRB), capillary ECs lack fenestrations, are joined by tight junctions, and are impermeable to serum constituents (4). Barrier competent CNS ECs express a distinctive set of plasma membrane pumps to actively extrude a wide variety of organic molecules and a distinctive set of transporters to facilitate CNS uptake of essential nutrients such as glucose. The physical and physiologic underpinnings of the BBB/BRB have been objects of fascination among biologists since their existence was first demonstrated by intravenous dye injection more than a century ago (4).

CNS vascular invasion and BBB development depend critically on canonical WNT signaling, as determined by eliminating WNT7a and WNT7b in the developing neuroepithelium and by eliminating or stabilizing β-catenin in ECs (5–7). In the retina and cerebellum, barrier integrity depends on Norrin, a TGF-β family member that is produced by glia and functions as a high-affinity WNT-like ligand for its EC receptor Frizzled4 (FZ4; refs. 8, 9). Mosaic deletion of FZ4 in mature retinal or cerebellar ECs leads to a cell-autonomous loss of the BRB or the BBB, respectively (10). Conversely, in mice lacking endogenous Norrin, initiating ectopic production of Norrin in adulthood restores BBB integrity in the cerebellum. Taken together, these data imply that BBB/BRB integrity depends on multiple canonical WNT signaling components and that this system remains plastic throughout life.

In addition to its role in CNS vascular integrity, Norrin/FZ4 signaling also plays a central role in retinal vascular growth. In mice, loss-of-function mutations in the genes coding for FZ4, Norrin, the coreceptor LDL receptor–related protein 5 (LRP5), or the integral membrane protein TSPAN12 lead to hypovascularization of the retina (8, 11–14). In humans, loss-of-function mutations in the X-linked Norrie disease gene (*NDP*, the gene coding for Norrin) causes severe hypovascularization of the retina, with persistence of the hyaloid vasculature, compensatory neovascularization, intraocular bleeding, retinal scarring, and blindness (15). Milder hypovascularization is associated with heterozygosity for mutations in *FZD4*, *LRP5*, and *TSPAN12* (16–20) and is referred to as familial exudative vitreoretinopathy (FEVR).

In the present paper, we address the role that different WNT signaling components play in BBB/BRB integrity and in retinal vascular development. We observe a variety of anatomic patterns and severities of BBB/BRB breakdown with different combinations of mutations in genes coding for WNT signaling components, imply-

Authorship note: Yulian Zhou, Yanshu Wang, and Max Tischfield are co–first authors.
Conflict of interest: The authors have declared that no conflict of interest exists.
Submitted: April 2, 2014; **Accepted:** June 12, 2014.
Reference information: *J Clin Invest*. 2014;124(9):3825–3846. doi:10.1172/JCI76431.

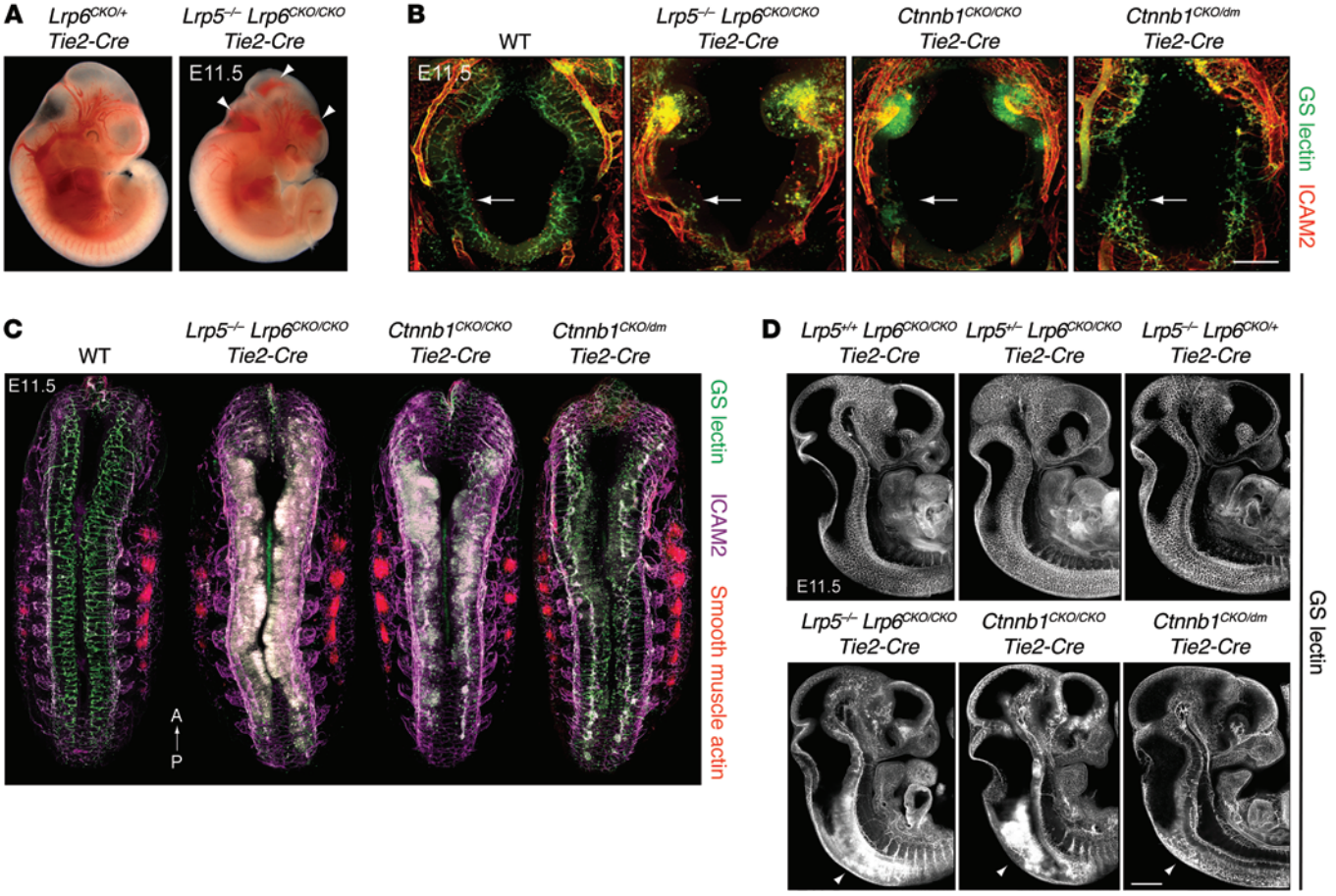

Figure 1. Effects of eliminating *Ctnnb1* or *Lrp5* and *Lrp6* in ECs on vascularization of the E11.5 CNS. (**A**) Bleeding in the hindbrain, midbrain, and forebrain of a *Lrp5*$^{-/-}$ *Lrp6*$^{CKO/CKO}$ *Tie2-Cre* embryo at E11.5 (arrowheads, right panel). Many embryos of this genotype also show bleeding in the spinal cord. Left, control embryo. (**B**) Transverse Z-stacked projections at E11.5 show severe vascularization defects in the *Lrp5*$^{-/-}$ *Lrp6*$^{CKO/CKO}$ *Tie2-Cre* and *Ctnnb1*$^{CKO/CKO}$ *Tie2-Cre* hindbrain and an intermediate vascularization defect in the *Ctnnb1*$^{CKO/dm}$ *Tie2-Cre* hindbrain (compare the regions highlighted by the arrows). Anti-ICAM2 stains ECs more strongly outside the CNS. GS lectin binds ECs and macrophages, which invade the hypovascularized CNS. Scale bar: 200 μm. (**C**) Spinal cord and hindbrain vascularization defects in E11.5 embryo whole mounts imaged from the dorsal surface. Z-stacks of approximately 70-μm thickness are shown. Smooth muscle actin highlights the somites. *Lrp5*$^{-/-}$ *Lrp6*$^{CKO/CKO}$ *Tie2-Cre* and *Ctnnb1*$^{CKO/CKO}$ *Tie2-Cre* embryos (center) show severe hypovascularization, formation of glomeruloid bodies, and bleeding within the spinal cord (white). The *Ctnnb1*$^{CKO/dm}$ *Tie2-Cre* embryo (far right) shows an intermediate vascularization defect. Anterior (A) is at the top; posterior (P) is at the bottom. (**D**) Optical sections in the sagittal plane of E11.5 embryos. The top 3 panels (*Lrp5*$^{+/+}$ *Lrp6*$^{CKO/CKO}$ *Tie2-Cre*, *Lrp5*$^{+/-}$ *Lrp6*$^{CKO/CKO}$ *Tie2-Cre*, and *Lrp5*$^{-/-}$ *Lrp6*$^{CKO/+}$ *Tie2-Cre*) show normal or nearly normal CNS vascularization. The left and middle bottom panels (*Lrp5*$^{-/-}$ *Lrp6*$^{CKO/CKO}$ *Tie2-Cre* and *Ctnnb1*$^{CKO/CKO}$ *Tie2-Cre*) show severe defects in CNS vascularization with bleeding that is most severe in the cervical spinal cord (arrowheads). The rightmost bottom panel (*Ctnnb1*$^{CKO/dm}$ *Tie2-Cre*) shows an intermediate vascularization defect in the spinal cord (arrowhead). Scale bar: 500 μm.

ing a previously unappreciated molecular heterogeneity within the CNS vasculature. We also provide strong evidence that Norrin/FZ4 signaling acts via the canonical WNT pathway by demonstrating that defects in *Ndp* or *Fz4* can be rescued by stabilizing β-catenin and can be phenocopied by ectopic expression of a dominant negative version of T cell factor-4 (TCF4).

Results

Varying severities of embryonic CNS vascularization defects with loss of canonical WNT signaling components. To extend earlier observations on the defects in embryonic CNS vascularization caused by EC-specific mutation of the β-catenin gene (*Ctnnb1*; refs. 5–7), we examined the phenotypes caused by partially or completely eliminating EC production of LRP5 and LRP6, the 2 closely related canonical WNT signaling coreceptors. Despite their functional and structural similarities, LRP5 and LRP6 play substantially different roles during development: *Lrp5*$^{-/-}$ mice are viable and fertile (21), whereas *Lrp6*$^{-/-}$ fetuses have multiple developmental defects that are incompatible with postnatal life (22). In these experiments, we have used a conventional *Lrp5* null allele and a conditional *Lrp6* allele (23) in combination with EC- and hematopoeitic stem cell–specific *Cre* expression (*Tie2-Cre*; ref. 24), and we have analyzed the phenotypes at E11.5, when CNS vascularization is well underway. At this age, no deleterious effect of gene knockout in hematopoeitic cells was seen.

Eliminating both LRP5 and LRP6 in ECs (*Lrp5*$^{-/-}$ *Lrp6*$^{CKO/CKO}$ *Tie2Cre*) has little effect on non-CNS vascular architecture, but led to severely attenuated CNS vascularization accompanied by cranial bleeding (Figure 1). The perineural vascular plexus lining the brain and spinal cord was hyperplastic, presumably second-

Table 1. Guide to genotypes, phenotypes, and figures

LOF or GOF alleles tested	Vascular development		Barrier formation		Figure[A]	
	Neural tube	Retina	Brain	Retina	Neural tube and brain	Retina
Ndp^{KO}	–	↓	↓	↓	3, 4, 7, 11, S4	6, 8, S5
Fz4^{KO}	–	↓	↓	↓	3, 4, 7, S1	6
Lrp5^{KO}	–	↓	–	↓	1, 2, 3, 4, S1	
Lrp6^{KO}	–	–	–	–	1	
Lrp5$^{+/-}$ *Lrp6*$^{-/-}$	–	–	–	–	1, 2	5
Lrp5$^{-/-}$ *Lrp6*$^{+/-}$	–	↓	–	↓	1, 2	5
Lrp5$^{-/-}$ *Lrp6*$^{-/-}$	↓	↓	↓	↓	1, 2	
Ctnnb1^{KO}	↓	↓	↓	↓	1, 2, 3, 4	5, 6, S3, S7
Ctnnb1^{dm}	↓	↓	↓	↓	1, 10	10, S7
Ctnnb1^{flex3}	ND	↑	↑	↑	7, 9	8, S5
TCF4^{KO}	–	–	–	↓		11, S8
dnTCF4	–	↓	↓	↓	11	11, S8

Genotypes analyzed in the figures are shown in the left column together with a summary assessment of the corresponding vascular phenotype for the mutant allele. KO refers to both conventional null alleles and condition KO alleles with Cre-mediated deletion. For many experiments, the KO was EC specific. Genotypes analyzed in Figure 3 and Supplemental Figure 1 are summarized in Figure 4. [A]S's indicate supplemental figures. Upward arrow, enhancement of normal vascular development or barrier function; downward arrow, suppression of normal vascular development or barrier function; horizontal line, no effect. LOF, loss of function; GOF, gain of function; ND, not determined.

ary to the failure of ECs to properly invade the neuroepithelium, and the few ECs that penetrated the neuroepithelium failed to remodel and instead formed clumps of ECs (glomeruloid bodies). This phenotype is identical to the phenotype observed with EC-specific loss of β-catenin (*Ctnnb1*$^{CKO/CKO}$ *Tie2-Cre*; Figure 1, B–D). Eliminating 2 or 3 of the 4 *Lrp* gene copies (*Lrp5*$^{+/+}$ *Lrp6*$^{CKO/CKO}$ *Tie2Cre*, *Lrp5*$^{+/-}$ *Lrp6*$^{CKO/CKO}$ *Tie2Cre*, or *Lrp5*$^{-/-}$ *Lrp6*$^{CKO/+}$ *Tie2Cre*) produced little or no effect on CNS vascularization, indicating that a single copy of either *Lrp5* or *Lrp6* suffices to support CNS vascular development at this age. We also tested the activity of a β-catenin derivative in which the transcriptional activation domains had been selectively disrupted (abbreviated "double mutant" [dm]; *Ctnnb1*^{dm}; ref. 25). Earlier work suggested that this derivative retains the capacity to associate with E-cadherin, and therefore it allows a distinction to be made between β-catenin's transcriptional and cell-junctional roles (25). At E11.5, *Ctnnb1*$^{CKO/dm}$ *Tie2-Cre* embryos showed a similar, although less severe, CNS vascularization defect compared with that seen in *Ctnnb1*$^{CKO/CKO}$ *Tie2-Cre* or *Lrp5*$^{-/-}$ *Lrp6*$^{CKO/CKO}$ *Tie2Cre* embryos (Figure 1, B–D), suggesting either that the *Ctnnb1*^{dm} allele retains some transcriptional activity and/or that β-catenin's cadherin-binding activity plays a minor role in embryonic CNS angiogenesis. Phenotypes produced by the *Ctnnb1*^{dm} allele at later times in development are described below. Table 1 provides a summary of the genotypes and phenotypes shown throughout the paper.

Widespread but nonuniform BBB defects in the adult brain with loss of Ctnnb1 or Lrp5 and Lrp6 in ECs. To extend the comparison between β-catenin and LRP5/LRP6 deficiency in ECs to the postnatal CNS vasculature, we used a *Pdgfb-CreER* transgene (26) to recombine the conditional alleles selectively in ECs after treatment with 4-hydroxytamoxifen (4HT). To incorporate a functional measure of BBB integrity, we examined leakage of the low molecular weight lysine-reactive biotinylation reagent sulfo–N-hydroxysuccinimide–biotin (sulfo-NHS-biotin) from the intravascular space into the brain parenchyma. WT, *Ctnnb1*$^{CKO/CKO}$ *Pdgfb-CreER*, and *Lrp5*$^{-/-}$ *Lrp6*$^{CKO/CKO}$ *Pdgfb-CreER* brains were analyzed at P23–P24, 1 week after 4HT treatment, or at P10, 2 days after 4HT treatment. (Early and efficient postnatal deletion of *Lrp5* and *Lrp6* or *Ctnnb1* in ECs led to death within approximately 3 days, thereby limiting the time window of the experiment and/or the 4HT dose that could be applied.) In WT controls, extensive leakage of sulfo-NHS-biotin occurred in and around the choroid plexus, the meninges, and the ventral hypothalamus, but the remaining brain parenchyma was protected by the BBB. In contrast, *Ctnnb1*$^{CKO/CKO}$ *Pdgfb-CreER* and *Lrp5*$^{-/-}$ *Lrp6*$^{CKO/CKO}$ *Pdgfb-CreER* brains showed widespread leakage in the striatum (arrows in Figure 2, A, F, and K), the paraventricular hypothalamus (arrows in Figure 2, B, G, and L), the ventral thalamus and cortex (arrows in Figure 2, C, H, and M), the pons and interpeduncular nuclei (arrows in Figure 2, D, I, and N), and the cerebellum and ventral brainstem (arrows in Figure 2, E, J, and O). Mural cell coverage was examined by antibody staining against PDGFRb and appeared essentially normal in affected regions (data not shown), supporting an EC-autonomous basis for the permeability defect. Brain regions with BBB defects also showed changes in EC protein composition consistent with a loss of barrier function. In particular, there was induction of plasmalemma vesicle–associated protein (PLVAP), a component of endothelial fenestrations (27), which is normally absent from CNS ECs, and repression of Claudin5, a tight junction protein. As seen in Figure 2, P–V, in regions with a leaky BBB, a subset of ECs had converted from a PLVAP$^-$Claudin5$^+$ state to a PLVAP$^+$Claudin5$^-$ state (arrow in Figure 2U), with the efficiency of conversion roughly correlated to the extent of sulfo-NHS-biotin leakage (Figure 2, P–U).

In the experiments in Figure 2, F–U, conversion of only a fraction of ECs to a BBB-deficient state was not unexpected: it presumably arose from incomplete recombination of the loxP targets by CreER. However, the regional variation in BBB breakdown in *Ctnnb1*$^{CKO/CKO}$ *Pdgfb-CreER* and *Lrp5*$^{-/-}$ *Lrp6*$^{CKO/CKO}$ *Pdgfb-CreER* brains was surprising. As seen in Figure 2, in both genotypes, the BBB was less affected in the dorsal, approximately 70% of the cortex, than in the ventral, 30%. Analogous regional differences were seen in the brain stem. Most striking was the high vascular permeability in the paraventricular hypothalamus, the pons, the interpeduncular nuclei, and the cerebellum relative to other brain regions. These observations imply that in the CNS vasculature at this age there are regional differences between ECs and/or their local environments.

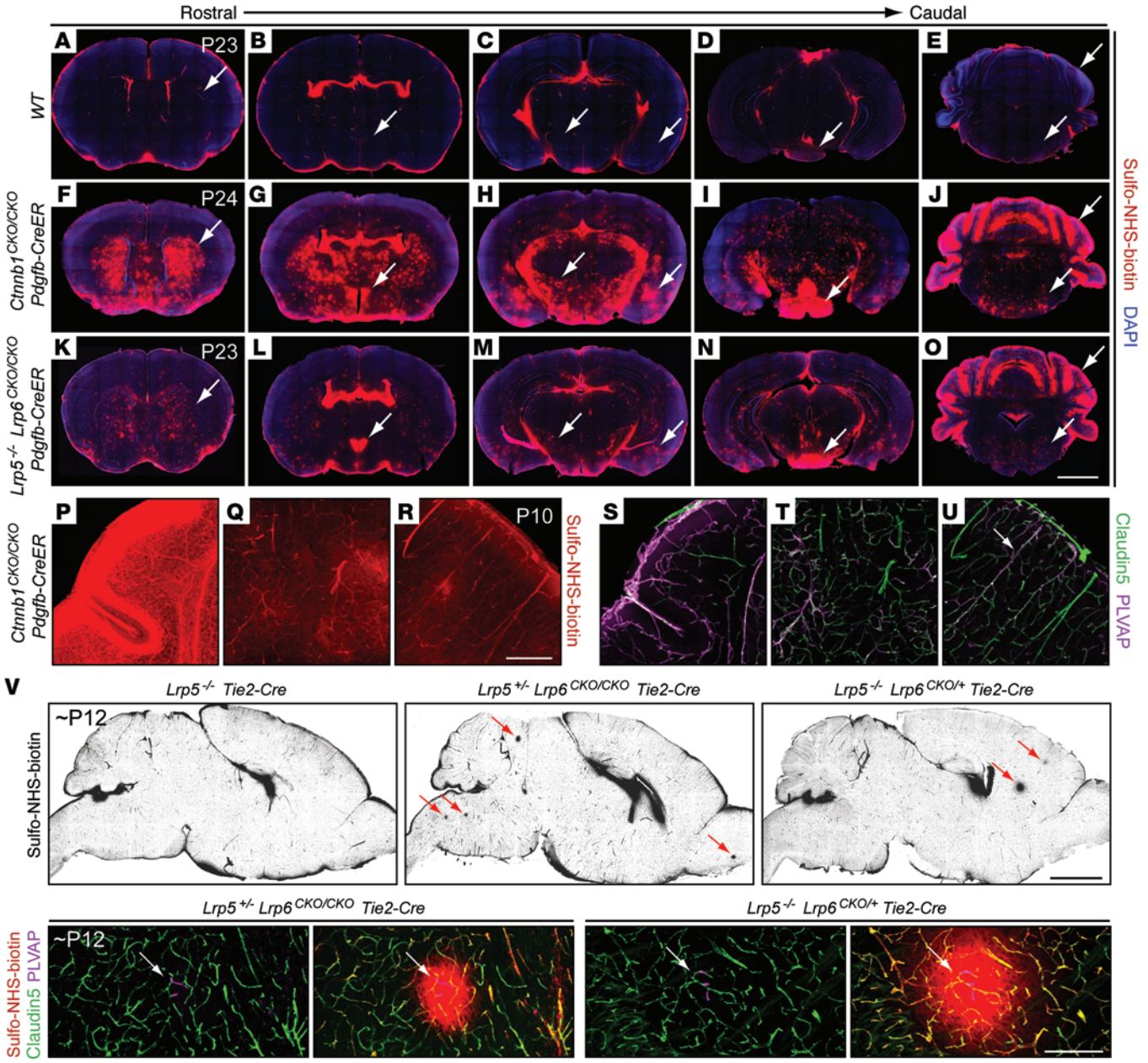

Figure 2. Effects of eliminating *Ctnnb1* or *Lrp5* and *Lrp6* postnatally in ECs. (**A**–**O**) Sulfo-NHS-biotin leakage in coronal sections from WT, *Lrp5*$^{-/-}$ *Lrp6*$^{CKO/CKO}$ *Pdgfb-CreER*, and *Ctnnb1*$^{CKO/CKO}$ *Pdgfb-CreER* brains at P23–P24, following 600 μg 4HT at P15 or 200 μg 4HT at P16. Leakage is seen around the choroid plexus, meninges, and ventral hypothalamus in all 3. In the *Lrp5*$^{-/-}$ *Lrp6*$^{CKO/CKO}$ *Pdgfb-CreER* and *Ctnnb1*$^{CKO/CKO}$ *Pdgfb-CreER* brains, scattered sites of leakage are seen in ventral cortex, striatum, thalamus, paraventricular hypothalamus, pons, brainstem, and cerebellum (arrows). Scale bar: 2 mm. (**P**–**U**) Sulfo-NHS-biotin leakage in a *Ctnnb1*$^{CKO/CKO}$ *Pdgfb-CreER* brain at P10, following 200 μg 4HT at P7. Leakage and PLVAP and Claudin5 immunostaining are shown in paired images from cerebellum (left panels), thalamus (center panels), and cortex (right panels). Leakage was most prominent in the cerebellum, with scattered sites of leakage in cortex and anterior thalamus. The conversion of ECs from PLVAP^{-}Claudin5^{+} to PLVAP^{+}Claudin5^{+} or PLVAP^{+}Claudin5^{-} roughly correlates with sites of leakage. Arrow in **U** points to a vessel that expresses PLVAP. Scale bar: 200 μm. (**V**) Sulfo-NHS-biotin leakage in P12 (approximately) *Lrp5*$^{-/-}$ *Tie2-Cre* (control), *Lrp5*$^{+/-}$ *Lrp6*$^{CKO/CKO}$ *Tie2-Cre*, and *Lrp5*$^{-/-}$ *Lrp6*$^{CKO/+}$ *Tie2-Cre* brains. There is no detectable leakage in *Lrp5*$^{-/-}$ *Tie2-Cre* brains (upper left) and there are rare foci of leakage (red arrows) in *Lrp5*$^{+/-}$ *Lrp6*$^{CKO/CKO}$ *Tie2-Cre* and *Lrp5*$^{-/-}$ *Lrp6*$^{CKO/+}$ *Tie2-Cre* brains (upper panels, center and right). Lower panels show rare foci of sulfo-NHS-biotin leakage are centered on small clusters of ECs that have converted to PLVAP^{+}Claudin5^{-} (arrows). In the left member of each image pair, the sulfo-NHS-biotin channel has been omitted. Scale bars: 2 mm (upper panels); 200 μm (lower panels).

These regional differences could reflect differences in the level of *Pdgfb-CreER* expression, accessibility of *loxP* targets, and/or the responses of ECs to loss of β-catenin or LRP5 and LRP6.

We next asked whether LRP5 and LRP6 act redundantly in the postnatal brain vasculature and whether a single functional *Lrp* allele (instead of the usual 4 alleles) could support BBB integrity. As seen in Figure 2V, *Lrp5*$^{+/-}$ *Lrp6*$^{CKO/CKO}$ *Tie2Cre* and *Lrp5*$^{-/-}$ *Lrp6*$^{CKO/+}$ *Tie2Cre* brains were vascularized normally with only rare foci of BBB breakdown that colocalize with sites where one or several capillary ECs had converted from a PLVAP^{-}Claudin5^{+}

to a PLVAP$^+$Claudin5$^-$ state. The extreme rarity of the converted EC clusters — on average several clusters per 120-μm–thick sagittal brain section — and the likely clonal relationship of the several ECs within each cluster suggest the possibility that each cluster arose from a rare somatic genetic or epigenetic event such as loss or inactivation of the single active *Lrp* allele. The plausibility of this conjecture rests on well-described mechanisms leading to rare somatic loss of tumor-suppressor gene function in premalignant cells (28). We conclude that a single copy of either *Lrp5* or *Lrp6* suffices to support postnatal vascular development and barrier integrity in the brain.

Distinctive anatomic distributions and severities of BBB defects in the postnatal brain with different combinations of Fz4, Ctnnb1, Lrp5, and Ndp mutations. In earlier work, we observed that a generalized loss of FZ4 or Norrin impairs vascular development and BBB integrity in the retina, cerebellum, and olfactory bulb, but not in the cerebral cortex or thalamus, and we and others observed that loss of LRP5 impairs vascular development only in the retina, suggesting that in different CNS regions, different combinations of Frizzled ligands (Norrin, WNT7a, WNT7b, etc.) and/or Frizzled receptors and coreceptors mediate canonical WNT signaling to promote vascular development and BBB integrity (10, 21). Defining the extent and anatomic distribution of BBB responses to perturbations in canonical WNT signaling could provide general insights into molecular and cellular heterogeneity within the CNS vasculature. As described above for *Lrp5*, *Lrp6*, and *Ctnnb1*, our approach has been to reduce or eliminate various combinations of canonical WNT-signaling components and then determine the territories in which BBB integrity is compromised, as judged by leakage of sulfo-NHS-biotin, induction of PLVAP expression, and loss of Claudin5 expression.

Since *Fz4* is expressed in all or nearly all CNS and non-CNS ECs (9), we asked whether a wider role for *Fz4* in BBB integrity could be revealed by eliminating *Fz4* on a genetic background that was sensitized by partial or complete loss of *Lrp5* or *Ctnnb1*. Eliminating 1 copy of *Fz4* in combination with *Lrp5* (*Fz4$^{CKO/+}$ Lrp5$^{-/-}$ Tie2Cre*; Figure 3A), 1 copy of *Ctnnb1* in combination with *Lrp5* (*Lrp5$^{-/-}$ Ctnnb1$^{CKO/+}$ Tie2Cre*; Figure 3F), or *Lrp5* alone (*Lrp5$^{-/-}$*; data not shown) had no apparent effect on BBB integrity. However, eliminating both copies of *Fz4* in combination with *Lrp5* (*Fz4$^{CKO/-}$ Lrp5$^{-/-}$ Tie2Cre*; Figure 3, B and E) greatly expanded the territories of BBB breakdown relative to that seen with elimination of *Fz4* alone (Figure 3C). In particular, P10–P11 *Fz4$^{CKO/-}$ Lrp5$^{-/-}$ Tie2Cre* mice showed zones of BBB breakdown in the thalamus, brain stem, cortex, and pons/interpeduncular nuclei (arrows in Figure 3, B and E). A somewhat different anatomic pattern was seen in *Fz4$^{CKO/-}$ Ctnnb1$^{CKO/+}$ Tie2Cre* mice: BBB breakdown was prominent in the pons/interpeduncular nuclei and cerebellum, but was not observed in the cortex, thalamus, or brain stem (Figure 3D).

In these experiments BBB loss was tightly correlated with the conversion of ECs from a PLVAP$^-$Claudin5$^+$ to a PLVAP$^+$Claudin5$^-$ state, as noted earlier in the context of Figure 2, P–U. We also observed a left-right mirror symmetry of BBB breakdown (e.g., Figure 3E), which implies a high degree of precision in the anatomic distribution of WNT activators and/or inhibitors in CNS tissue or in the abundance and composition of WNT-signaling components in the CNS vasculature.

Consistent with the comparison between *Fz4$^{CKO/+}$ Lrp5$^{-/-}$ Tie2-Cre* and *Fz4$^{CKO/-}$ Lrp5$^{-/-}$ Tie2-Cre* brains (Figure 3, A and B), a more extensive allelic series (*Fz4$^{CKO/+}$ Tie2-Cre*, *Fz4$^{CKO/+}$ Lrp5$^{-/-}$ Tie2-Cre*, *Fz4$^{CKO/-}$ Tie2-Cre*, and *Fz4$^{CKO/-}$ Lrp5$^{-/-}$ Tie2-Cre*) showed a progressive increase in PLVAP in cerebellar ECs and a corresponding decline in cerebellar BBB integrity, with a progressive reduction in the number of functional *Fz4* and/or *Lrp5* alleles (Supplemental Figure 1; supplemental material available online with this article; doi:10.1172/JCI76431DS1). A graded phenotypic effect was also seen in the context of kidney growth when *Lrp5$^{-/-}$ Fz4$^{+/+}$*, *Lrp5$^{-/-}$ Fz4$^{+/-}$*, and *Lrp5$^{-/-}$ Fz4$^{-/-}$* embryos were compared (Supplemental Figure 2), consistent with a sensitizing effect of *Lrp5* loss and analogous to the kidney growth phenotypes observed previously with loss of both *Fz4* and *Fz8* (29). These data indicate that loss of *Fz4* and *Lrp5* synergize in both CNS ECs and in kidney development.

Ndp (the gene encoding Norrin) is expressed by glia throughout the CNS: in Bergman glia in the cerebellum, Muller glia in the retina, and astrocytes in other CNS regions (30). However, mutation of *Ndp* produces only a relatively mild loss of BBB integrity that is confined to the cerebellum and olfactory bulb (10). To explore the possibility that Norrin might function more widely — but redundantly — with other Frizzled ligands, we examined the effect of *Ndp* mutation on BBB integrity in genetic backgrounds that were sensitized by heterozygous loss of *Fz4* or homozygous loss of *Lrp5*. (*Ndp* is an X-linked gene. To simplify the text that follows, we refer to both *Ndp$^{-/-}$* females and *Ndp$^{-/Y}$* males as *Ndp^{KO}*.) *Ndp^{KO} Fz4$^{+/-}$* mice showed more extensive disruption of the cerebellar BBB than *Ndp^{KO}* mice, but the BBB defects did not extend to other CNS regions (Figure 3, G and H),and *Ndp^{KO} Lrp5$^{-/-}$* mice showed an even greater disruption of the cerebellar BBB, with additional BBB defects in the brain stem and thalamus (Figure 3I). (As noted above in the context of Supplemental Figure 1, heterozygous loss of *Fz4* or complete loss of *Lrp5* cause no defects in the cerebellar BBB.) The latter observation implies a wider role for Norrin in BBB integrity than had previously been appreciated based only on the *Ndp^{KO}* phenotype.

The results of the postnatal BBB experiments are shown in semiquantitative form in Figure 4. For each of 5 brain regions (cerebral cortex, thalamus, pons/interpeduncular nuclei, brainstem, and cerebellum), the extent of BBB compromise has been scored as absent, mild, moderate, or severe. Experiments utilizing *Pdgfb-CreER*–mediated recombination (Figure 2) have not been included in this figure because in those experiments the severity of BBB dysfunction depended on 4HT dose and cannot be compared directly to the severities observed with conventional null alleles or constitutively recombined conditional alleles. Figure 4 shows a broad trend in which the pons, interpeduncular nuclei, and cerebellum are most sensitive to loss of canonical WNT signaling genes, the brainstem and thalamus are of intermediate sensitivity, and the cortex is least sensitive.

Lrp5 plays a major role and Lrp6 plays a minor role in retinal vascular development. To determine the relative importance of LRP5 and LRP6 in retinal vascular development, we compared the anatomy, BRB integrity, and molecular phenotype of the retinal vasculature in *Lrp5$^{+/-}$ Lrp6$^{CKO/CKO}$ Tie2Cre* and *Lrp5$^{-/-}$ Lrp6$^{CKO/+}$ Tie2Cre* mice. In P12 *Lrp5$^{+/-}$ Lrp6$^{CKO/CKO}$ Tie2Cre* retinas, the vascular architecture was indistinguishable from that of WT (Figure 5A). In con-

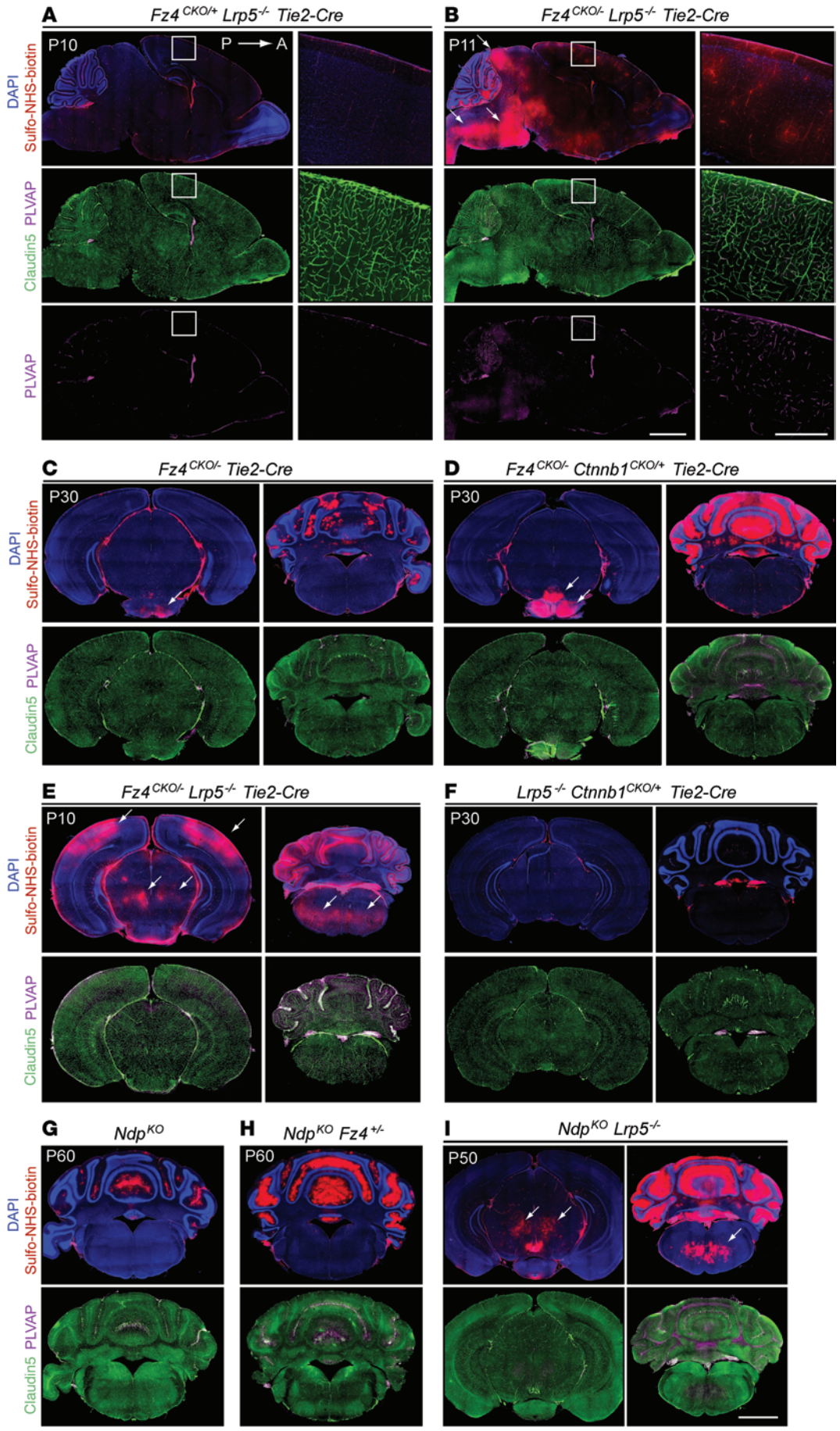

Figure 3. Distinctive severities and locations of BBB defects in mice with different combinations of loss-of-function mutations in canonical WNT signaling components. (**A**–**I**) Representative brain sections showing sulfo-NHS-biotin leakage and Claudin5 and PLVAP immunostaining. (**A** and **B**) Sagittal sections near the midline (with boxed regions enlarged to the right). (**C**–**I**) Coronal sections. (**C**–**F** and **I**) Thalamus and cortex (left panels) and cerebellum and brainstem (right panels). (**G** and **H**) Cerebellum and brainstem. In **C**–**I**, the high degree of left-right symmetry in sulfo-NHS-biotin leakage implies a nonrandom distribution of BBB loss. In all sections, territories with the greatest PLVAP induction also exhibit the greatest BBB loss. Arrows highlight some of the regions with BBB breakdown. In **A** and **B**, anterior (A) is to the right and posterior (P) is to the left. Scale bars: 2 mm (low magnification), 500 μm (high magnification) (**A** and **B**); 2 mm (**C**–**I**).

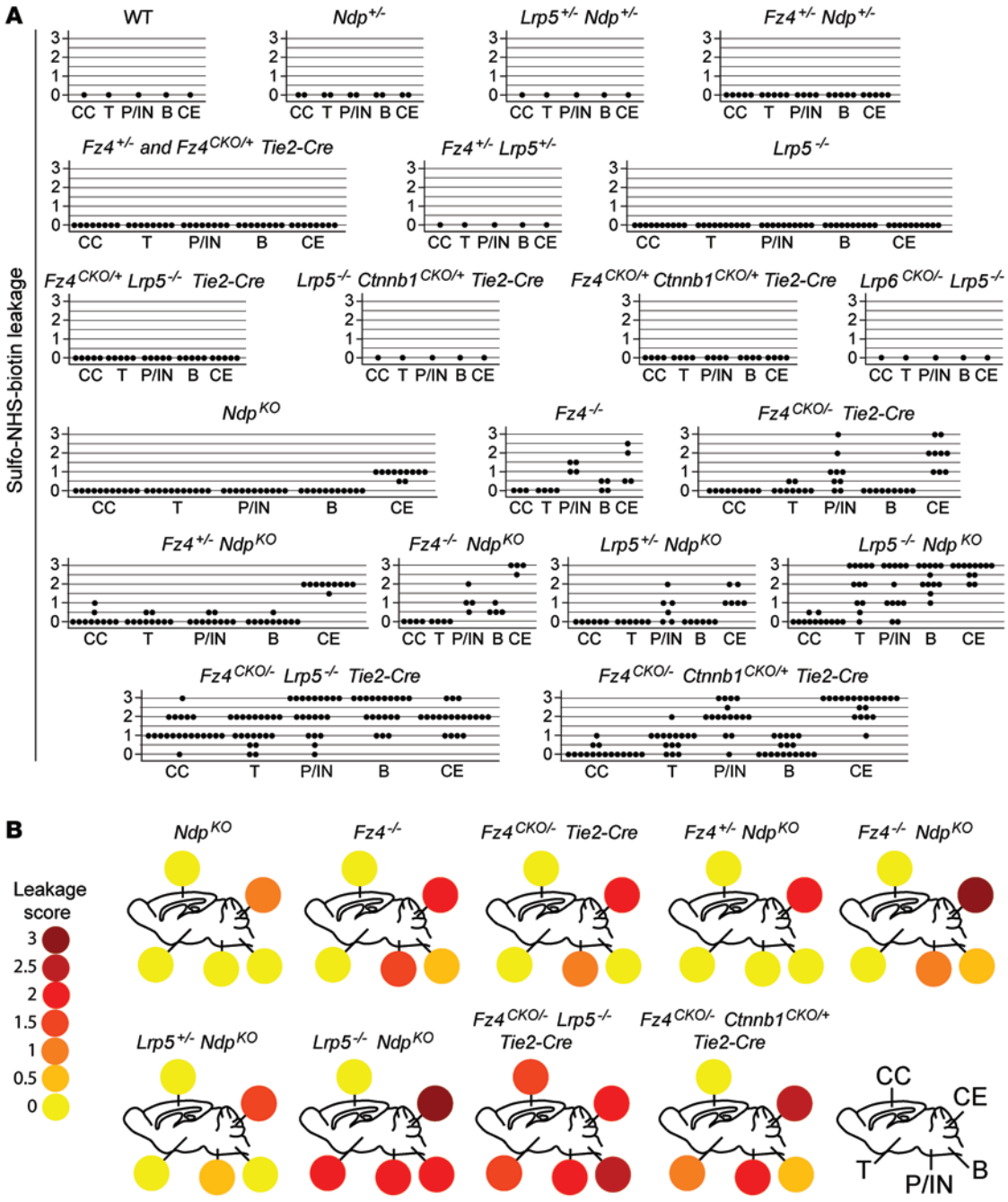

Figure 4. Semiquantitative analysis of the locations and severities of postnatal BBB defects, based on sulfo-NHS-biotin leakage, with different combinations of loss-of-function mutations in canonical WNT signaling components. (**A**) BBB defects were scored as absent (0), mild (1), moderate (2), or severe (3) in the cerebral cortex, thalamus, pons/interpeduncular nuclei, brain stem, and cerebellum. Each circle represents the assessment for a single mouse for each of the 5 indicated brain regions. Only brains from P10 or older mice were scored. CC, cerebral cortex; T, thalamus; P/IN, pons/interpeduncular nuclei; B, brainstem; CE, cerebellum. (**B**) Color-coded summary of mean BBB defect scores (from part **A**) for each brain region and genotype. The colors represent the severity of the BBB defect, as summarized by the 0 to 3 leakage score described for **A**.

trast, in P12 *Lrp5*$^{-/-}$ *Lrp6*$^{CKO/+}$ *Tie2Cre* retinas, there was a paucity of deep capillaries, a conversion of all ECs to a PLVAP^{+}Claudin5^{-} phenotype, and multiple zones of BRB breakdown (Figure 5A), a phenotype that closely resembles the *Lrp5*$^{-/-}$ phenotype (12, 31). Earlier comparisons of *Fz4*$^{-/-}$, *Ndp*^{KO}, and *Lrp5*$^{-/-}$ retinal vascular phenotypes showed that *Lrp5*$^{-/-}$ retinas exhibit a slightly milder vascular invasion defect, consistent with a model in which LRP6 plays a minor role in retinal ECs (9). The observations in Figure 5A support that model and further show that in the absence of *Lrp6*, a single copy of *Lrp5* suffices for retinal vascular development. The comparison between *Lrp5*$^{+/-}$ *Lrp6*$^{CKO/CKO}$ *Tie2Cre* and *Lrp5*$^{-/-}$ *Lrp6*$^{CKO/+}$ *Tie2Cre* phenotypes in the retina stands in sharp contrast to the same comparison in the embryonic neuroepithelium and postnatal brain (Figure 1D and Figure 2V), where a single copy of

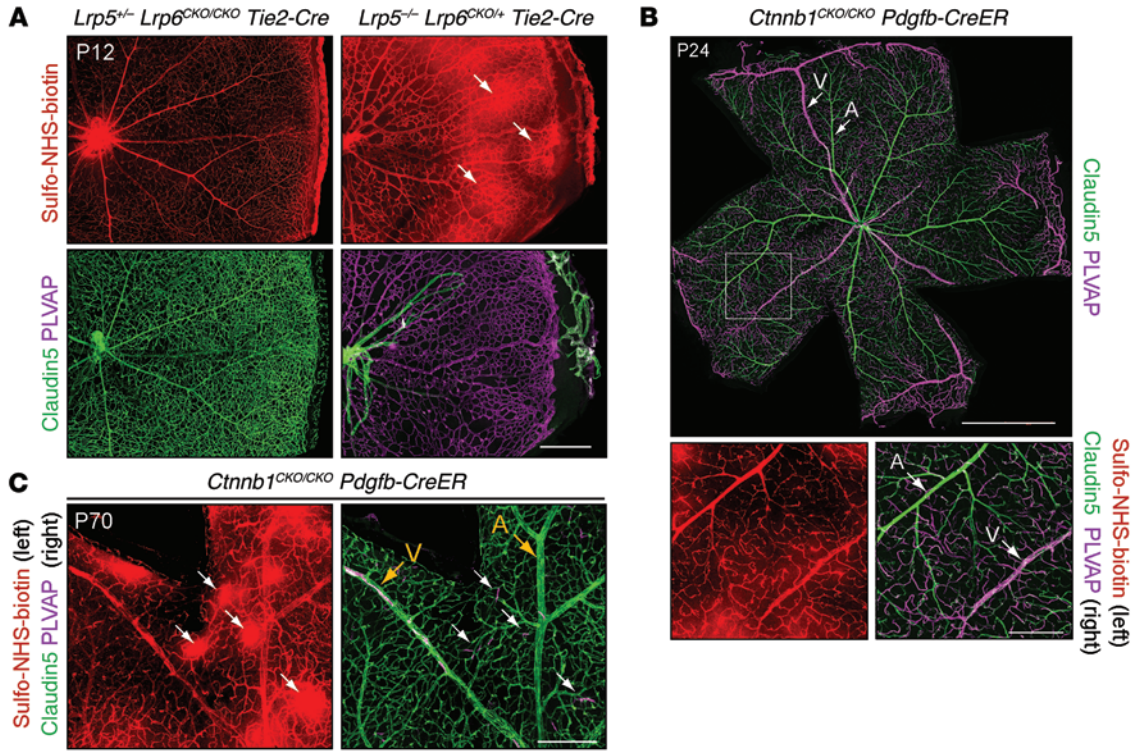

Figure 5. Differential effects of eliminating *Ctnnb1* and *Lrp5* versus *Lrp6* on brain versus retina ECs and on retinal artery versus vein/capillary ECs. (**A**) P12 *Lrp5*$^{+/-}$ *Lrp6*$^{CKO/CKO}$ *Tie2-Cre* and *Lrp5*$^{-/-}$ *Lrp6*$^{CKO/+}$ *Tie2-Cre* retinas showing no vascular phenotype with 1 functional copy of *Lrp5* and no functional copies of *Lrp6* (left) and a nearly complete conversion of retinal ECs from PLVAP$^-$Claudin5$^+$ to PLVAP$^+$Claudin5$^-$ with no functional copies of *Lrp5* and 1 functional copy of *Lrp6* (right). The truncated PLVAP$^-$Claudin5$^+$ vessels emanating from the optic disc in the *Lrp5*$^{-/-}$ *Lrp6*$^{CKO/+}$ *Tie2-Cre* retina are hyaloid arteries. Scattered foci of sulfo-NHS-biotin leakage are present in the *Lrp5*$^{-/-}$ *Lrp6*$^{CKO/+}$ *Tie2-Cre* retina (white arrows). Scale bar: 500 μm. (**B**) P24 *Ctnnb1*$^{CKO/CKO}$ *Pdgfb-CreER* retina from a mouse that had received 200 μg 4HT at P17. Efficient conversion of ECs from PLVAP$^-$Claudin5$^+$ to PLVAP$^+$Claudin5$^-$ is seen in capillaries and veins, but not in arteries. The boxed region in the upper panel is enlarged in the 2 lower panels. A, artery; V, vein. Scale bar: 1 mm. (**C**) P70 *Ctnnb1*$^{CKO/CKO}$ *Pdgfb-CreER* retina from a mouse that had received 200 μg 4HT at P55. Rare conversions of retinal ECs from PLVAP$^-$Claudin5$^+$ to PLVAP$^+$Claudin5$^-$ are seen in capillaries and veins (yellow arrow), but not in arteries (yellow arrow) and correspond to sites of sulfo-NHS-biotin leakage (white arrows). Scale bar: 200 μm.

either *Lrp5* or *Lrp6* fully supported normal vascular development and integrity. Thus, the relative roles played by LRP5 and LRP6 in vascularization and barrier formation differ substantially between the retina and other CNS regions.

Differences in the sensitivity of arterial, vein, and capillary ECs in the retina to loss of canonical WNT-signaling components. To completely eliminate canonical WNT signaling in retinal ECs during defined time windows, *Ctnnb1*$^{CKO/CKO}$ *Pdgfb-CreER* mice were treated with 4HT at ages ranging from P10 to approximately P60. When canonical WNT signaling was eliminated in ECs during a 2-day window from P5 to P7, PLVAP was induced in retinal ECs, but Claudin5 levels showed little change (data not shown), most likely due to the perdurance of Claudin5 protein and/or mRNA. When canonical WNT signaling was eliminated in ECs during a 2-day window from P10 to P12 or during a 7-day window from P17 to P24, the PLVAP$^+$Claudin5$^-$ state was confined to vein and capillary ECs (Figure 5B and Supplemental Figure 3), suggesting that arterial ECs attain a state of differentiation that makes their PLVAP$^-$Claudin5$^+$ status impervious to decrements in canonical WNT signaling. (We note that an alternative explanation for this result is that there is a selective repression of the *Pdgfb-CreER* transgene or a selective inaccessibility of the *Ctnnb1*^{CKO} target in arterial ECs. This alternative explanation, at least as applied to *CreER* expression, is unlikely because we have measured the 4HT-induced Cre activity of *Pdgfb-CreER* at P14–P16 using a Cre-activated nuclear *tdTomato* reporter knocked into the *Hprt* locus [*Hprt*$^{LSL\text{-}tdT}$; ref. 32] and observed a uniformly high efficiency of recombination in arterial, capillary, and vein ECs [data not shown].)

With increasing age, 4HT treatment of mature retinas converted fewer ECs to a PLVAP$^+$Claudin5$^-$ state. This age-dependent decline could reflect a decline in accessibility of *loxP* targets with increasing age (a trend that is seen with many conditional alleles), or alternately it could represent a progressive decline in the plasticity of the EC state. The converted ECs were confined to veins and capillaries, where they were associated with sulfo-NHS-biotin leakage (Figure 5C). Cre-mediated recombination of *Ctnnb1*$^{CKO/CKO}$ after P15 had no obvious effect on retinal vascular architecture. The conversion of some adult retinal ECs to a PLVAP$^+$Claudin5$^-$ state provides further evidence for ongoing canonical WNT signaling in the mature CNS vasculature.

Varying severities of retinal vascular growth and BRB defects with loss of different canonical WNT-signaling components. In a strategy analogous to that shown in Figure 3, we examined the retinal vascular phenotypes that resulted from mutating different combina-

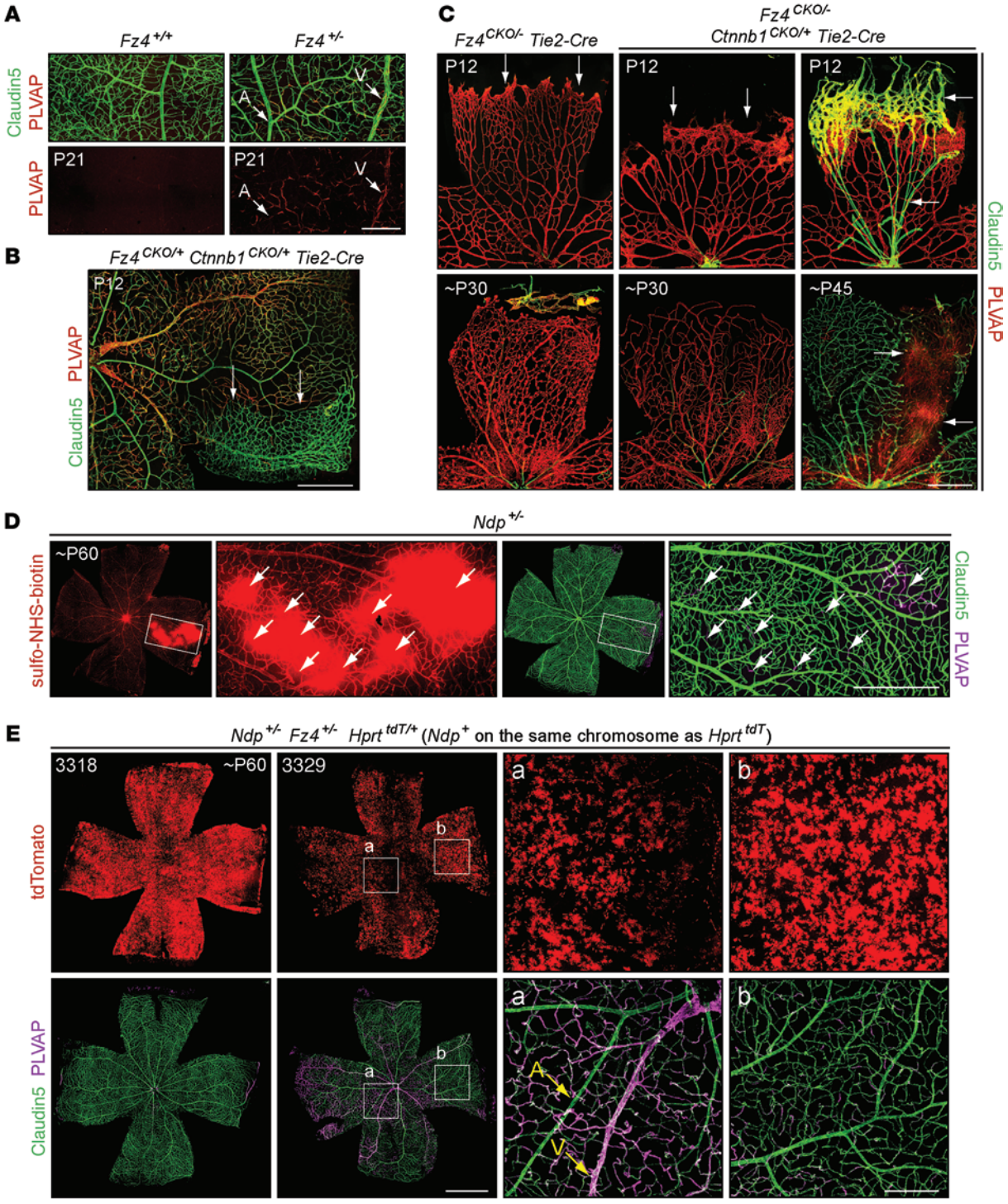

Figure 6. Vascular growth and BRB defects in retinas with different combinations of loss-of-function mutations in canonical WNT signaling components. (**A**) PLVAP expression in capillary and vein ECs in *Fz4*$^{+/-}$ but not *Fz4*$^{+/+}$ retinas. Scale bar: 200 μm. (**B**) Mosaic recombination in *Fz4*$^{CKO/+}$ *Ctnnb1*$^{CKO/+}$ *Tie2-Cre* retinas: recombined territory (upper two-thirds) with enhanced PLVAP and reduced Claudin5 in veins and capillaries and reduced vascular density, and unrecombined territory (arrows) with PLVAP^{-}Claudin5^{+} ECs and normal vascular density. Scale bar: 500 μm. (**C**) More severe vascular defects in *Fz4*$^{CKO/-}$ *Ctnnb1*$^{CKO/+}$ *Tie2-Cre* (right 4 panels) compared with *Fz4*$^{CKO/-}$ *Tie2-Cre* retinas (left 2 panels). Scale bar: 500 μm. (**D**) Representative flat-mount retina from an adult *Ndp*$^{+/-}$ female. Rare PLVAP^{+}Claudin5^{-} ECs (arrows) are associated with sulfo-NHS-biotin leakage. Boxed regions in low-magnification panels are enlarged to the right. Scale bar: 500 μm. (**E**) Compared with *Ndp*$^{+/-}$ retinas (e.g., **D**), approximately 50% of adult *Fz4*$^{+/-}$ *Ndp*$^{+/-}$ retinas show more extensive conversion of ECs from to a PLVAP^{+}Claudin5^{-} state. The *Hprt*^{tdT} reporter and the *Ndp*$^{+}$ allele are on the same X chromosome, and the *Ndp*$^{-}$ allele is on the unmarked X chromosome. tdTomato shows the pattern of X chromosome mosaicism. Retina 3318 shows few PLVAP^{+}Claudin5^{-} ECs. Retina 3329a shows multiple territories with a high density of PLVAP^{+}Claudin5^{-} ECs. Boxed regions marked a (low density of *Ndp*$^{+}$ cells) and b (high density of *Ndp*$^{+}$ cells) are enlarged at right. Scale bars: 1 mm (left panels); 200 μm (right panels).

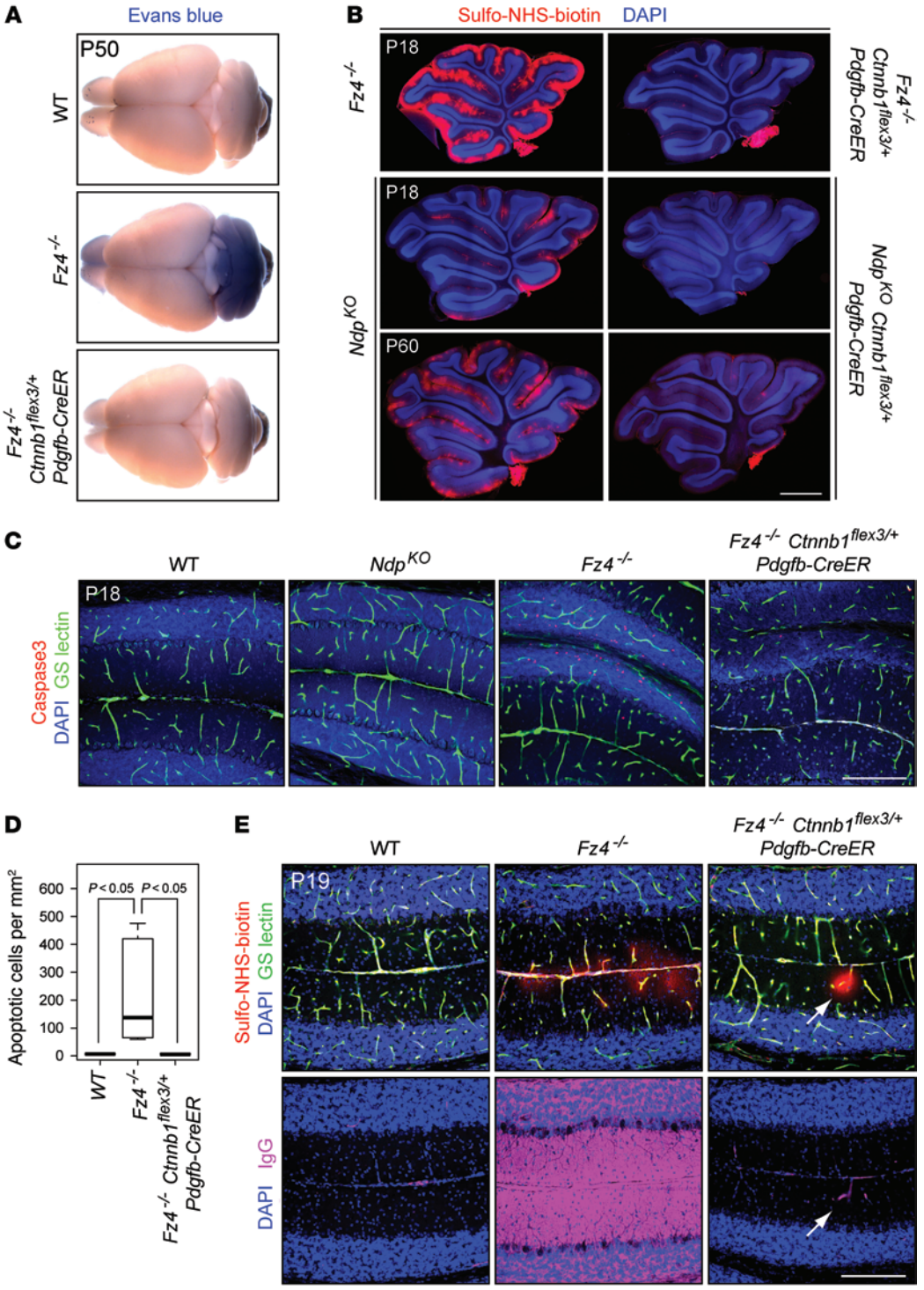

Figure 7. Production of stabilized β-catenin in ECs rescues *Ndp*^{KO} and *Fz4*$^{-/-}$ cerebellar BBB defects. (**A**) BBB integrity assessed by i.p. injection of Evans blue at P50. Brains were collected 1 day after Evans blue injection. *Fz4*$^{-/-}$ *Ctnnb1*$^{flex3/+}$ *Pdgfb-CreER* mice received 4 i.p. injections of a total of 330 μg 4HT/injection between P10 and P45. (**B**) Cerebellar BBB integrity assessed by sulfo-NHS-biotin leakage in *Fz4*$^{-/-}$ and *Ndp*^{KO} mice (left panels) and *Fz4*$^{-/-}$ *Ctnnb1*$^{flex3/+}$ *Pdgfb-CreER* and *Ndp*^{KO} *Ctnnb1*$^{flex3/+}$ *Pdgfb-CreER* mice (right panels). β-Catenin stabilization rescues the cerebellar BBB defect. In **B**–**E**, mice carrying the *Ctnnb1*^{flex3} *Pdgfb-CreER* allele received 3 to 4 i.p. injections of 20 to 100 μg 4HT/injection at intervals of 2 to 3 days between P2 and P10, a regimen that leads to nearly complete EC recombination of the *Ctnnb1*^{flex3} allele in the presence of *Pdgfb-CreER*. Scale bar: 1 mm (**B**). (**C** and **D**) Neuronal death, measured by cleaved caspase 3 immunostaining, is abundant in the *Fz4*$^{-/-}$ cerebellum and is suppressed in the *Fz4*$^{-/-}$ *Ctnnb1*$^{flex3/+}$ *Pdgfb-CreER* cerebellum at P18. Box and whisker plot parameters are described in Methods. Scale bar: 200 μm. (**E**) BBB integrity assessed by extravasation of mouse IgG and by sulfo-NHS-biotin leakage in WT, *Fz4*$^{-/-}$, and *Fz4*$^{-/-}$ *Ctnnb1*$^{flex3/+}$ *Pdgfb-CreER* cerebella at P19. Although β-catenin stabilization largely rescues the cerebellar BBB defect, rare sites of leakage remain (arrows, right panels). Scale bar: 200 μm.

tions of WNT-signaling components. Phenotypes associated with loss of 1 *Fz4* allele are of special interest because heterozygous loss of *Fz4* is a common cause of FEVR (19). Although the *Fz4*$^{+/-}$ retinal vasculature was architecturally normal, a minority of capillary and vein — but not arterial — ECs had converted to a PLVAP^{+}Claudin5^{-} state (Figure 6A). In contrast to the retina, a single copy of *Fz4* was sufficient to suppress PLVAP expression throughout the brain vasculature (data not shown). A retinal and brain EC phenotype nearly identical to that seen in *Fz4*$^{+/-}$ mice was observed in *Ctnnb1*$^{+/-}$ mice (data not shown). The variable conversion of retinal ECs implies that halving the *Fz4* or *Ctnnb1* gene dosage brings retinal ECs close to a threshold for conversion between mutually exclusive developmental states, one PLVAP^{-}Claudin5^{+} and the other PLVAP^{+}Claudin5^{-}. This represents the first observation, to our knowledge, of a phenotypic alteration in an animal model with a genotype that matches one of the genotypes responsible for FEVR. It suggests that conversion of human retinal ECs to a PLVAP^{+}Claudin5^{-} state may represent the fundamental cellular defect in FEVR.

Although retinas heterozygous for loss of *Fz4* or *Ctnnb1* show little or no change in vascular architecture, when the 2 mutations were combined, the retinal vascular architecture was clearly abnormal. Figure 6B shows an unusual and especially informative $Fz4^{CKO/+}$ $Ctnnb1^{CKO/+}$ *Tie2Cre* retina with variegated expression of *Tie2Cre*. In the phenotypically WT territory (arrows), either $Fz4^{CKO}$ or $Ctnnb1^{CKO}$ or both have failed to recombine, and, as a result, the vasculature is architecturally normal and ECs are PLVAP$^-$Claudin5$^+$. The remainder of the image shows the typical $Fz4^{CKO/+}$ $Ctnnb1^{CKO/+}$ *Tie2Cre* retinal vascular phenotype, with reduced vascular density and partial conversion of many ECs to a PLVAP$^+$Claudin5$^-$ state.

If FZ4 were the only receptor responsible for canonical WNT signaling in retinal ECs, then one would predict that the $Fz4^{-/-}$ phenotype in the retina would be indistinguishable from the most severe phenotype produced by loss-of-function mutations in canonical WNT-signaling components. To test this idea, we asked whether eliminating *Fz4* and simultaneously halving the level of β-catenin leads to a retinal vascular phenotype that is more severe than that seen in $Fz4^{-/-}$ mice. An affirmative answer would imply that Frizzled family members other than FZ4 also play a role in retinal vascular development. Figure 6C shows a comparison between $Fz4^{CKO/-}$ *Tie2-Cre* and $Fz4^{CKO/-}$ $Ctnnb^{CKO/+}$ *Tie2-Cre* retinas at P12 and at P30–P45. In mice of both genotypes, the superficial vasculature is unable to productively invade the retina, generating instead a large number of glomeruloid structures. Interestingly, the P12 $Fz4^{CKO/-}$ $Ctnnb^{CKO/+}$ *Tie2-Cre* vasculature shows sparser coverage and retarded radial growth relative to the $Fz4^{CKO/-}$ *Tie2-Cre* vasculature (vertical arrows in Figure 6C). By way of comparison, in WT retinas, the vasculature completely covers the retina by approximately P8 (data not shown). In some $Fz4^{CKO/-}$ $Ctnnb^{CKO/+}$ *Tie2-Cre* retinas at approximately P12, the periphery is densely vascularized by an in-growth from the hyaloid vasculature (horizontal arrows in the P12 retina in Figure 6C), a pattern that is only rarely seen in $Fz4^{-/-}$ retinas. The large-diameter PLVAP$^-$Claudin5$^+$ hyaloid vessels originate at the optic disc, grow radially over the surface of the retina, and form a dense arbor in the region of peripheral retina that is not covered by the intrinsic retinal vasculature. This growth of hyaloid-derived vessels likely reflects a response to severe hypoxia in the retinal periphery. In the P45 retina shown in Figure 6C, a fully recombined territory (horizontal arrows) with PLVAP$^+$Claudin5$^-$ ECs and a high-surface vascular density — presumably a secondary response to retinal hypoxia — is contrasted with the adjacent unrecombined territory, which is populated by PLVAP$^-$Claudin5$^+$ ECs at normal vascular density. In summary, the greater severity of the $Fz4^{CKO/-}$ $Ctnnb^{CKO/+}$ *Tie2-Cre* retinal vascular phenotype compared with the $Fz4^{CKO/-}$ *Tie2-Cre* phenotype suggests that additional receptors — presumably other Frizzled family members — may play at least a minor role in canonical WNT signaling in retinal ECs.

Retinal vascular phenotypes in Ndp and Fz4 double heterozygotes. The X-chromosomal location of *Ndp* provides an opportunity to examine variation in Norrin action in $Ndp^{+/-}$ females due to variation in the topography of X chromosome inactivation (XCI). In female mouse retinas, contiguous territories that express one or the other X chromosome generally vary from tens to hundreds of microns in diameter (32, 33). In earlier work with $Ndp^{+/-}$ females, in which the topography of the XCI mosaic was visualized with a constitutively expressed X-linked tdTomato reporter ($Hprt^{tdT}$), we observed a subset of retinas with unusually coarse XCI mosaicism in which PLVAP$^+$Claudin5$^-$ vasculature showed a high spatial correlation with regions of retinal parenchyma expressing the Ndp^{KO} allele (32).

To extend the observations of Wu et al. (32), we examined retinas that combined heterozygosity for *Ndp* with a sensitized genetic background in which *Fz4* gene dosage was halved ($Ndp^{+/-}$ $Fz4^{+/-}$). Typically, $Ndp^{+/-}$ retinas exhibit only a few highly localized regions of BRB deficiency, and these correspond to the locations of small numbers of ECs — or even single ECs — that are PLVAP$^+$Claudin5$^-$ (Figure 6D). In contrast, in approximately half of the $Ndp^{+/-}$ $Fz4^{+/-}$ retinas, there were large numbers of PLVAP$^+$Claudin5$^-$ ECs that covered contiguous territories of up to several hundred microns (Figure 6E), a far greater size and density of PLVAP$^+$Claudin5$^-$ ECs than were found in $Fz4^{+/-}$ retinas or in $Ndp^{+/-}$ retinas (compare Figure 6E, panel a, with Figure 6A). In $Ndp^{+/-}$ $Fz4^{+/-}$ retinas, PLVAP$^+$Claudin5$^-$ ECs were present in regions with the lowest density of retinal cells expressing the Ndp^+ (i.e., $Hprt^{tdT}$) X chromosome. These data imply that in $Ndp^{+/-}$ mice, Norrin levels in many regions of the retina are only marginally above the threshold for maintaining ECs in a PLVAP$^-$Claudin5$^+$ state, and this near-threshold level is revealed by halving the FZ4 level. If the same situation holds in humans, then genetic background differences that modulate canonical WNT signaling might be expected to produce phenotypic heterogeneity among *NDP* carrier females.

β-catenin stabilization rescues brain and retinal vascular defects caused by mutation of Fz4 or Ndp. Norrin shows no sequence homology or structural similarity to the WNT family of proteins (34, 35). However, in transfected HEK/293 cells, Norrin, FZ4, LRP5, and Tspan12 activate canonical WNT signaling (8, 13), and the general assumption in the field has been that the roles of these proteins in retinal vascular development involve only this pathway (14). In addition to the canonical WNT pathway, 2 noncanonical pathways are also able to transmit signals from Frizzled receptors and could potentially play a role in EC development and homeostasis: the WNT/Ca^{++} pathway, which is hypothesized to involve Frizzled activation of a G-protein (36), and the planar cell polarity (PCP) pathway, which relays signals from asymmetrically localized cell-surface complexes to the cytoskeleton (37). The possibility that Norrin and FZ4 signal via pathways other than the canonical WNT pathway has been raised by 2 recent studies, one suggesting that FZ4 regulates arterial development via noncanonical WNT/PCP signaling (38) and the second suggesting that, in addition to its role as a FZ4 ligand, Norrin also acts as a bone morphogenetic protein (BMP) antagonist (39).

To test the hypothesis that the canonical WNT pathway is the principal or only signaling pathway that is affected by loss of Norrin or FZ4 in vivo, we first asked whether EC induction of a canonical WNT signaling reporter transgene, *Tcf/Lef-lacZ* (*BAT-gal*; ref. 40), differed between WT and Ndp^{KO} retinas and cerebella. Immunostaining for the nuclear-localized β-galactosidase reporter showed approximately 2-fold and approximately 5-fold reductions in the number of β-galactosidase–positive EC nuclei in P4–P5 Ndp^{KO} cerebella and retinas, respectively, a difference that was easily detected despite the substantial variegation in transgene expression (Supplemental Figure 4). Next we asked whether artificially stabilizing β-catenin in ECs could rescue the CNS vascular phenotypes in $Fz4^{-/-}$ and Ndp^{KO} mice. As β-catenin is downstream

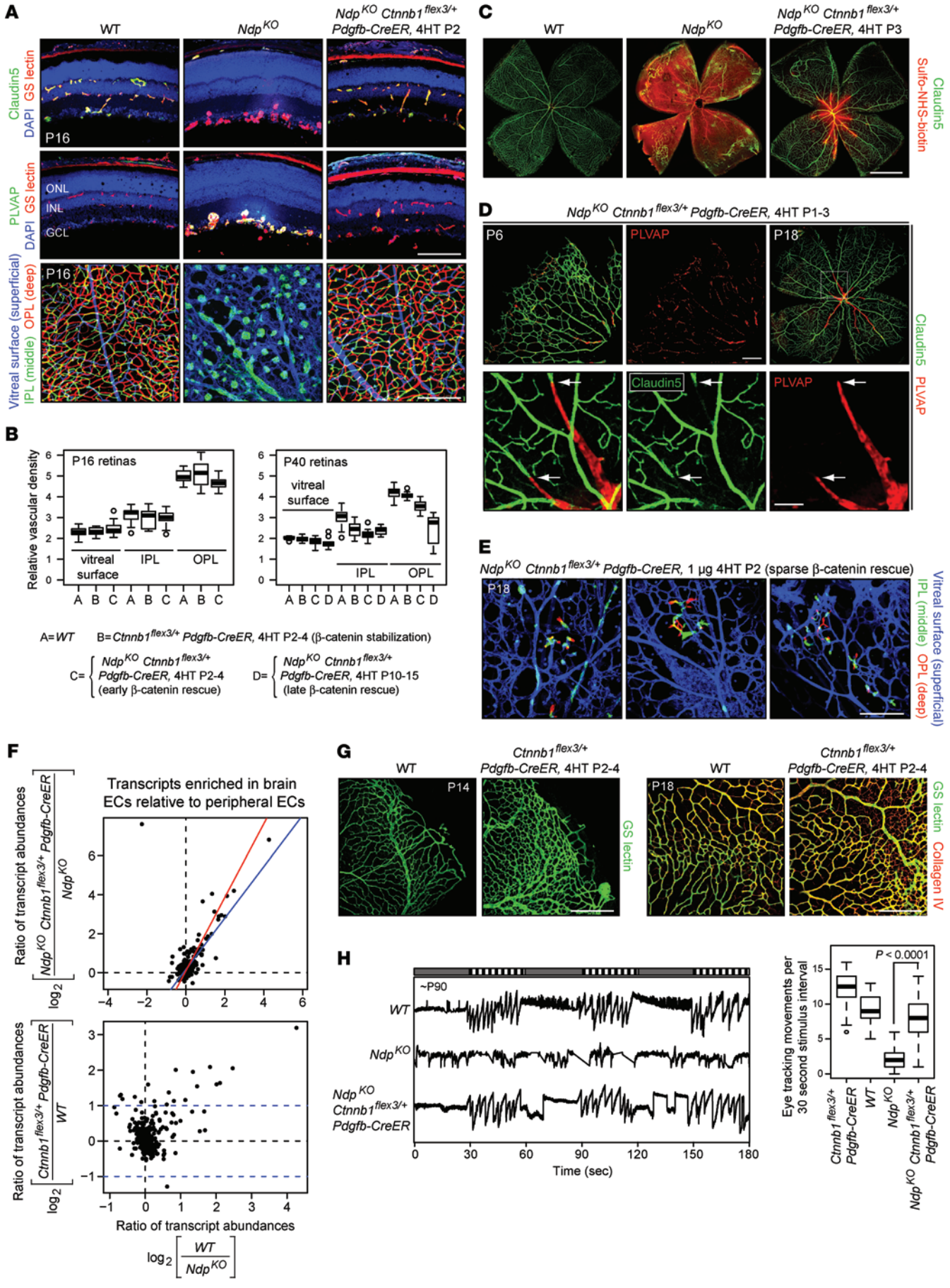
A
WT
Ndp^KO
Ndp^KO Ctnnb1^flex3/+ Pdgfb-CreER, 4HT P2
Claudin5 GS lectin DAPI
P16
PLVAP GS lectin DAPI
ONL
INL
GCL
Vitreal surface (superficial) IPL (middle) OPL (deep)
B
Relative vascular density
P16 retinas
P40 retinas
vitreal surface
IPL
OPL
A=WT
B=Ctnnb1^flex3/+ Pdgfb-CreER, 4HT P2-4 (β-catenin stabilization)
C= Ndp^KO Ctnnb1^flex3/+ Pdgfb-CreER, 4HT P2-4 (early β-catenin rescue)
D= Ndp^KO Ctnnb1^flex3/+ Pdgfb-CreER, 4HT P10-15 (late β-catenin rescue)
C
WT
Ndp^KO
Ndp^KO Ctnnb1^flex3/+ Pdgfb-CreER, 4HT P3
Claudin5 Sulfo-NHS-biotin
D
Ndp^KO Ctnnb1^flex3/+ Pdgfb-CreER, 4HT P1-3
P6
PLVAP
P18
Claudin5
PLVAP
E
Ndp^KO Ctnnb1^flex3/+ Pdgfb-CreER, 1 µg 4HT P2 (sparse β-catenin rescue)
P18
Vitreal surface (superficial) IPL (middle) OPL (deep)
F
Transcripts enriched in brain ECs relative to peripheral ECs
Ratio of transcript abundances log2 [Ndp^KO Ctnnb1^flex3/+ Pdgfb-CreER / Ndp^KO]
Ratio of transcript abundances log2 [Ctnnb1^flex3/+ Pdgfb-CreER / WT]
Ratio of transcript abundances log2 [WT / Ndp^KO]
G
WT
Ctnnb1^flex3/+ Pdgfb-CreER, 4HT P2-4
P14
P18
GS lectin Collagen IV
H
~P90
WT
Ndp^KO
Ndp^KO Ctnnb1^flex3/+ Pdgfb-CreER
Time (sec)
Eye tracking movements per 30 second stimulus interval
P < 0.0001
Ctnnb1^flex3/+ Pdgfb-CreER
WT
Ndp^KO
Ndp^KO Ctnnb1^flex3/+ Pdgfb-CreER

Figure 8. Production of stabilized β-catenin in ECs rescues *Ndp*^{KO} retinal vascular defects. (**A**) Retinal vasculature at P16 in WT, *Ndp*^{KO}, and *Ndp*^{KO} *Ctnnb1*$^{flex3/+}$ *Pdgfb-CreER* mice treated with 20 μg 4HT at P2. Cross sections (upper) and flat mounts (lower; vascular depth color-coded). GCL, ganglion cell layer; ONL, outer nuclear layer. Scale bars: 200 μm. (**B**) Vascular density at P16 and P40. Box and whisker plot parameters; see Methods. (**C**) BRB integrity assessed by sulfo-NHS-biotin leakage in adult WT, *Ndp*^{KO}, and *Ndp*^{KO} *Ctnnb1*$^{flex3/+}$ *Pdgfb-CreER* retinas. *Ndp*^{KO} *Ctnnb1*$^{flex3/+}$ *Pdgfb-CreER* mice were treated with 20 μg 4HT at P3. Scale bar: 1 mm. (**D**) Retinas from *Ndp*^{KO} *Ctnnb1*$^{flex3/+}$ *Pdgfb-CreER* mice treated with 20 μg 4HT at P2–P3. White arrows, boundary between PLVAP$^+$Claudin5$^-$ and PLVAP$^-$Claudin5$^+$ territories. Scale bars: 200 μm. (**E**) Flat-mount retinas from *Ndp*^{KO} *Ctnnb1*$^{flex3/+}$ *Pdgfb-CreER* mice treated with 1 μg 4HT at P2. Depth is color coded. Scale bar: 200 μm. (**F**) Whole P10 retina RNAseq from WT, *Ndp*^{KO}, *Ctnnb1*$^{flex3/+}$ *Pdgfb-CreER*, and *Ndp*^{KO} *Ctnnb1*$^{flex3/+}$ *Pdgfb-CreER* mice treated with 20 μg 4HT at P3. Upper panel, ratios of transcript abundances: *Ndp*^{KO} *Ctnnb1*$^{flex3/+}$ *Pdgfb-CreER* versus *Ndp*^{KO} (*y* axis) and WT versus *Ndp*^{KO} (*x* axis). Least squares regression line (blue; R^2 = 0.62) and orthogonal (Deming) regression (red; ref. 69). Lower panel, ratios of transcript abundances: *Ctnnb1*$^{flex3/+}$ *Pdgfb-CreER* versus WT (*y* axis) and WT versus *Ndp*^{KO} (*x* axis). (The upper left point is likely an artifact and was not included in the line fitting, and the upper right point was also omitted from the line fitting so that it would not dominate the regression calculation). (**G**) Peripheral retinas of WT and *Ctnnb1*$^{flex3/+}$ *Pdgfb-CreER* mice treated with 50 to 100 μg 4HT at P2–P4. Scale bars: 200 μm. (**H**) Left panel, horizontal eye position during OKR representative recordings. Right panel, OKR quantification. *n* = 3 or more mice per genotype.

of the Norrin/FZ4/LRP complex at the plasma membrane and is the sole conduit of the canonical WNT signal from cytoplasm to nucleus, and as β-catenin stabilization appears to play no role in noncanonical WNT signaling or BMP signaling, this experiment should provide a clear test of the hypothesis. In these experiments, β-catenin stabilization was effected by Cre-mediated deletion of *Ctnnb1* exon 3, which codes for sites of GSK3 phosphorylation that promote β-catenin ubiquitination and degradation (41). We note that the amino acids coded by *Ctnnb1* exon 3 appear to be dispensable for β-catenin's transcriptional regulatory activity and also that exon 3 is a multiple of 3 nucleotides in length so that its removal does not introduce a frame shift.

As shown in Figure 7, A and B, β-catenin stabilization produced a nearly complete rescue of the *Fz4*$^{-/-}$ and *Ndp*^{KO} cerebellar BBB phenotypes, as determined by both Evans blue and sulfo-NHS-biotin leakage. Coincident with restoration of BBB integrity, we observed an abrogation of apoptotic death among cerebellar granule cells in *Fz4*$^{-/-}$ *Ctnnb1*$^{flex3/+}$ *Pdgfb-CreER* mice (Figure 7, C and D). Close inspection of cerebella from *Fz4*$^{-/-}$ *Ctnnb1*$^{flex3/+}$ *Pdgfb-CreER* mice that had received high-dose 4HT at P2–P10, showed only rare vascular segments that were permeable to endogenous mouse IgG and sulfo-NHS-biotin (Figure 7E). These segments presumably represent rare ECs in which CreER-mediated recombination of the *Ctnnb1*^{flex3} allele did not occur.

When *Ndp*^{KO} *Ctnnb1*$^{flex3/+}$ *Pdgfb-CreER* mice were injected with 4HT on or before P3 ("early β-catenin rescue"), we observed vascular invasion of the retina, the formation of a capillary plexus on either side of the inner nuclear layer (INL), and a restoration of the PLVAP$^-$Claudin5$^+$ EC state (Figure 8A). When these retinas were examined at P16, the vascular anatomy differed from that of the WT only by a small reduction in capillary density in the outer plexiform layer (OPL) (Figure 8B). Treatment with 4HT at P10–P15 ("late β-catenin rescue") — an age when vascular invasion is well under way in WT retinas and is severely retarded in *Ndp*^{KO} retinas — resulted in nearly complete rescue of the inner plexiform layer (IPL) plexus but only partial rescue of the OPL plexus (Figure 8B). Finally, treatment with 4HT at P21–P25, after the completion of retinal vascular development, resulted in partial restoration of Claudin5 expression in veins and capillaries and a large increase in the number of intraretinal glomeruloid structures, which did not produce an intraretinal capillary plexus (Supplemental Figure 5). Thus, the extent of anatomic rescue depends in a graded manner on the timing of the canonical WNT signal.

Interestingly, in adult *Ndp*^{KO} *Ctnnb1*$^{flex3/+}$ *Pdgfb-CreER* retinas treated with 4HT at P3, the central approximately 1 mm of each radial vein displayed the *Ndp*^{KO} phenotype, both molecularly and functionally: PLVAP was expressed, Claudin5 was repressed, and intravascular sulfo-NHS-biotin leaked through the endothelium (Figure 8, C and D). We ascribe this distinctive topography to 2 factors: the radial migration of ECs during normal retinal development and the retarded migration and delayed proliferation of ECs that lack Norrin/FZ4 signaling (9, 10). If, as seems likely, CreER-mediated recombination of the *Ctnnb1*^{flex3} allele was incomplete after a single dose of 4HT, then the early postnatal *Ndp*^{KO} *Ctnnb1*$^{flex3/+}$ *Pdgfb-CreER* retinal vasculature would have consisted of a mixed population of defective and rescued ECs. Since the rescued ECs would be expected to proliferate and migrate more efficiently than the defective ECs, the result would be a mature retinal vasculature in which the periphery is populated largely or exclusively by rescued ECs. The data in Figure 8, C and D, indicate that ECs that lack Norrin/FZ4 signaling are at a competitive disadvantage with respect to both proliferation and migration.

A variation on the preceeding *Ctnnb1*^{flex3} rescue experiment revealed the invasive properties of small numbers of rescued ECs. When *Ndp*^{KO} *Ctnnb1*$^{flex3/+}$ *Pdgfb-CreER* mice were given a very low

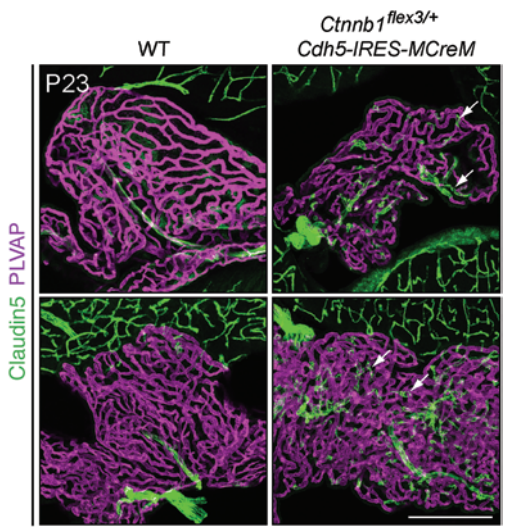

Figure 9. EC expression of stabilized β-catenin produces a cell-autonomous conversion of choroid plexus ECs from PLVAP$^+$Claudin5$^-$ to PLVAP$^-$Claudin5$^+$. *Ctnnb1*$^{flex3/+}$ *Cdh5-IRES-MCreM* mice were treated with 200 μg 4HT at P3 and analyzed at P23. Two images are shown per genotype. White arrows point to a few of the several dozen choroid plexus capillary ECs per image that have converted to a PLVAP$^-$Claudin5$^+$ state. Scale bar: 200 μm.

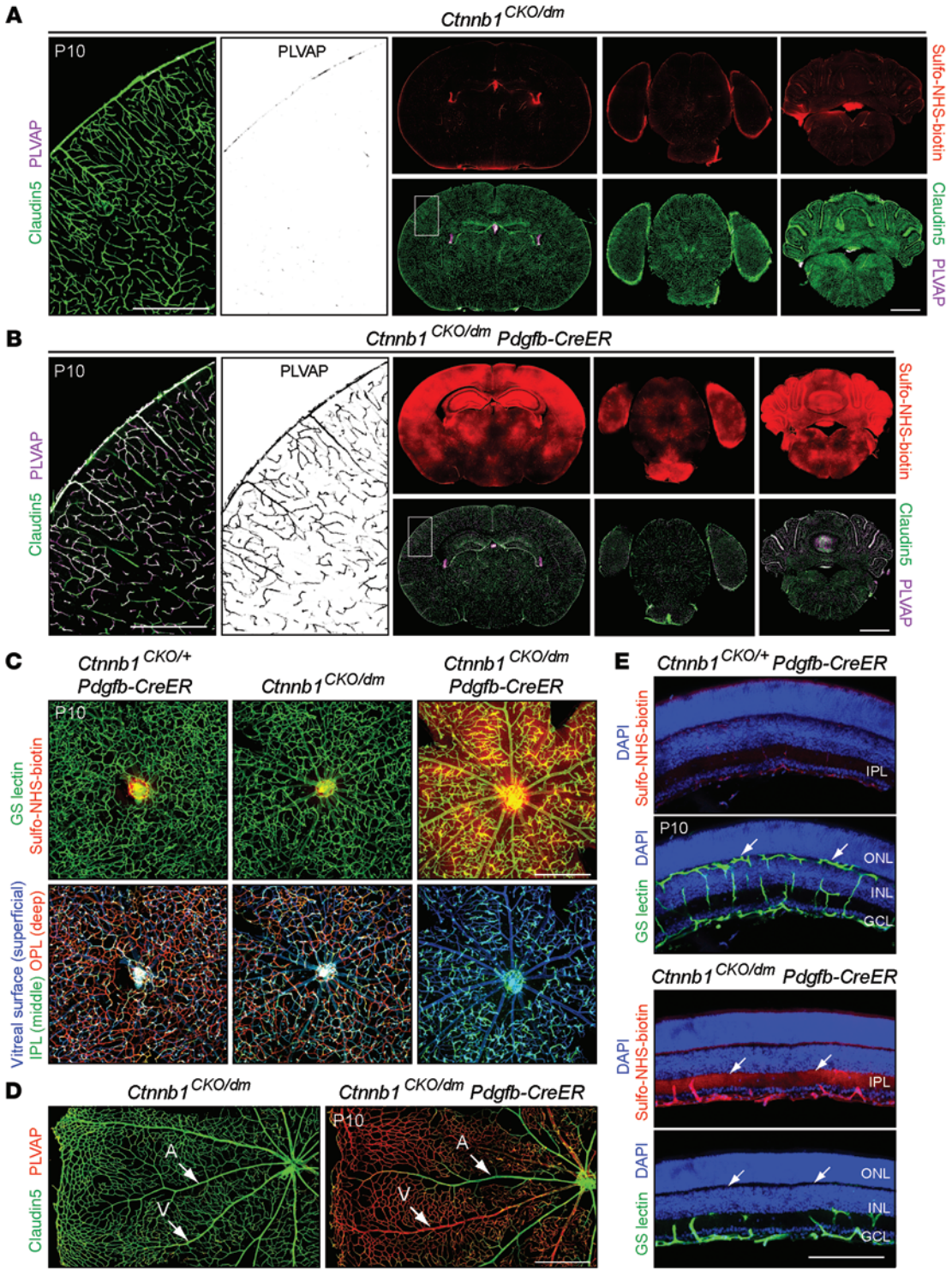

Figure 10. Transcriptionally inactive β-catenin cannot support normal retinal vascular development and BBB/BRB integrity. (**A** and **B**) Brains from P10 *Ctnnb1*$^{CKO/dm}$ (control) and *Ctnnb1*$^{CKO/dm}$ *Pdgfb-CreER* mice treated with 60 μg 4HT at P6. Right panels, coronal sections at the anterior hippocampus (left), the pons (center), and the cerebellum (right). Enlarged images (left) show Claudin5 and PLVAP in the cerebral cortical vasculature, corresponding to the white rectangles (center). *Ctnnb1*$^{CKO/dm}$ brains show PLVAP$^-$Claudin5$^+$ vasculature and no sulfo-NHS-biotin leakage. *Ctnnb1*$^{CKO/dm}$ *Pdgfb-CreER* vasculature shows many PLVAP$^+$Claudin5$^-$ ECs and extensive sulfo-NHS-biotin leakage. Scale bars: 500 μm (left panels); 2 mm (right panels). (**C**) Flat-mount retinas from P10 *Ctnnb1*$^{CKO/+}$ *Pdgfb-CreER*, *Ctnnb1*$^{CKO/dm}$, and *Ctnnb1*$^{CKO/dm}$ *Pdgfb-CreER* mice treated with 50 to 100 μg 4HT at P6. Upper row, the BRB is compromised in *Ctnnb1*$^{CKO/dm}$ *Pdgfb-CreER* retinas. Bottom row, retinal vasculature color coded by depth. *Ctnnb1*$^{CKO/dm}$ *Pdgfb-CreER* retinas have far fewer deep retinal capillaries. Scale bar: 400 μm. (**D**) Flat-mount retinas from P10 *Ctnnb1*$^{CKO/dm}$ (control) and *Ctnnb1*$^{CKO/dm}$ *Pdgfb-CreER* mice treated with 60 μg 4HT at P6. *Ctnnb1*$^{CKO/dm}$ *Pdgfb-CreER* retinas show efficient conversion of vein and capillary ECs from PLVAP$^-$Claudin5$^+$ to PLVAP$^+$Claudin5$^-$. Low levels of PLVAP in *Ctnnb1*$^{CKO/dm}$ capillaries are due to heterozygosity for *Ctnnb1*. Scale bar: 500 μm. (**E**) Cross sections of P10 retinas from control *Ctnnb1*$^{CKO/+}$ *Pdgfb-CreER* (upper panels) and *Ctnnb1*$^{CKO/dm}$ *Pdgfb-CreER* mice (lower panels) treated with 50 to 100 μg 4HT at P6. *Ctnnb1*$^{CKO/dm}$ *Pdgfb-CreER* retinas show extensive vascular leakage in the IPL (arrows in the Sulfo-NHS-biotin panel) and lack deep retinal capillaries (arrows in the GS-lectin panels). Scale bar: 200 μm.

dose (~1 μg) of 4HT at P2–P4 and their retinas examined at P18, multiple well-separated clusters of ECs were found within the retina from the vitreal surface to the IPL and OPL (Figure 8E). It seems likely that each cluster arose from a single rescued EC and that this cell and its progeny were able to carry out the normal vascular invasion program.

The transcriptional response to Norrin/FZ4 signaling has been studied previously by analyzing whole retinas and immunoaffinity-purified vascular cells (9, 31). To assess the extent to which β-catenin stabilization in the Ndp^{KO} background restored normal EC gene expression, total retina RNA from P10 WT, Ndp^{KO}, $Ctnnb1^{flex3/+}$ *Pdgfb-CreER*, and Ndp^{KO} $Ctnnb1^{flex3/+}$ *Pdgfb-CreER* mice was subjected to RNAseq and the abundances of brain EC-enriched transcripts - a set defined by transcriptome profiling of FACS sorted CNS vs. peripheral ECs (42) — were compared across genotypes (Supplemental Tables 1–4; RNAseq data has been deposited in the NCBI's [GEO GSE56461]). To minimize transcriptome differences that might reflect cellular responses to 4HT exposure, all of the mice were treated with approximately 20 μg 4HT at P3. As seen in the upper panel of Figure 8F, Ndp^{KO} retinas rescued with stabilized β-catenin showed transcript abundance changes relative to Ndp^{KO} retinas that largely parallel the changes observed when WT is compared with Ndp^{KO} retinas. A smaller positive correlation was observed in comparing stabilized β-catenin versus WT and WT versus Ndp^{KO} (Figure 8F). Similar trends were seen when the transcriptome was expanded to include differentially expressed transcripts in a brain EC versus neuron/glia comparison (Supplemental Figure 6 and ref. 42). Transcripts coding for Sox17, a transcription factor previously shown to be induced in ECs by FZ4 signaling (9, 10, 43), were induced 6.6-fold in Ndp^{KO} $Ctnnb1^{flex3/+}$ *Pdgfb-CreER* compared with Ndp^{KO} retinas and 3.2-fold in $Ctnnb1^{flex3/+}$ *Pdgfb-CreER* compared with WT retinas. Taken together, these experiments imply that stabilized β-catenin largely restores the WT profile of the EC transcriptome to Ndp^{KO} ECs.

The small number of transcript abundance changes induced by stabilization of β-catenin on a WT background ($Ctnnb1^{flex3/+}$ *Pdgfb-CreER*; Figure 8F), appeared to have little effect on vascular architecture in $Ctnnb1^{flex3/+}$ *Pdgfb-CreER* retinas. The densities of all 3 layers of vasculature were close to normal at P40 (Figure 8B), although at earlier times, there was an increase in vascular density at the retinal periphery followed by an increase in empty collagen IV sleeves, an indicator of increased vessel remodeling (Figure 8G). The data suggest that homeostatic mechanisms largely compensated for the gene expression changes caused by constitutive activation of the canonical WNT signaling pathway in ECs.

Ndp^{KO} and $Fz4^{-/-}$ mice lack an ERG b-wave and have little or no image-forming vision, as assessed by the optokinetic response (OKR) (ref. 9). To test the extent of functional rescue by β-catenin stabilization, we compared OKR responses between WT, Ndp^{KO}, $Ctnnb1^{flex3/+}$ *Pdgfb-CreER*, and Ndp^{KO} $Ctnnb1^{flex3/+}$ *Pdgfb-CreER* mice, all treated with 5 to 10 μg 4HT at P2–P4. Figure 8H shows that early stabilization of β-catenin largely rescued the OKR defect, consistent with the anatomic rescue of the retinal vasculature. The OKR responses of rescued mice were more variable than those of the WT controls (Figure 8H), most likely due to the variable extent of rescue of the vascular anatomy. Most or all of the "eye-tracking movements" in Ndp^{KO} mice appear to be random saccades unrelated to the moving visual stimulus; for consistency, they have been counted in the quantification in Figure 8H.

In sum, the phenotypic rescue by stabilized β-catenin supports the hypothesis that Norrin/FZ4 signaling influences retinal and cerebellar vascular development and barrier formation largely — and perhaps exclusively — via the canonical WNT-signaling pathway.

β-catenin stabilization converts the molecular properties of high permeability ECs in the choroid plexus to a more BBB-like state. Liebner et al. (5) showed that stabilizing β-catenin in prenatal mouse brain ECs in vivo or in adult mouse brain ECs in culture promotes expression of BBB markers and EC barrier properties, and Stenman et al. (6) showed that non-CNS ECs in mid-gestation embryos could be induced to express a BBB marker (glucose transporter Glut-1) by ectopic WNT7a expression. Here, we have asked whether ECs within a mature high-permeability vascular bed can be reconfigured to a more BBB-like state by inducing canonical WNT signaling. We focused on the choroid plexus because this vasculature expresses high levels of PLVAP and exhibits high permeability, essential features for the production of cerebrospinal fluid from a plasma filtrate.

To ensure that Cre-mediated recombination occurred only in response to 4HT injection, this experiment required a CreER driver free of background recombination in the absence of 4HT. As *Pdgfb-CreER* gives a low level of background recombination with a variety of reporters (data not shown), we constructed a *VE-cadherin* (*Cdh5*) knockin allele in which an internal ribosome entry site (*IRES*) was followed by a *Cre* open-reading frame fused on both 5′ and 3′ sides to DNA coding for mouse estrogen receptor ligand-binding domains that preferentially recognize 4HT (*Mer-Cre-Mer* or *MCreM*). The presence of 2 ER domains in the *MCreM* fusion protein substantially reduces background Cre-mediated recombination relative to the levels seen with the single ER domain in conventional CreER proteins, most likely because 4HT-independent recombination arises from rare proteolytic cleavage events that liberate the Cre domain from the ER domain that maintains cytoplasmic retention (44). In the *Cdh5-IRES-MCreM* allele, the *IRES* sequence reduces translation of the *MCreM* protein, further lowering Cre activity. Preliminary experiments showed that mice carrying both *Cdh5-IRES-MCreM* and a highly recombinogenic *loxP* reporter ($Hprt^{LSLtdT}$; ref. 32) exhibited no reporter-expressing cells in the absence of 4HT (data not shown).

The choroid plexus develops prenatally, achieving its mature ultrastructure by the time of birth (45). When $Ctnnb1^{flex3/+}$ *Cdh5-IRES-MCreM* mice were treated with 200 μg 4HT at P3 and the choroid plexus examined at P23, approximately 5% to 10% of capillary ECs had converted from $PLVAP^{+}Claudin5^{-}$ to $PLVAP^{-}Claudin5^{+}$, whereas age-matched controls showed a choroid plexus in which the capillary ECs were uniformly $PLVAP^{+}Claudin5^{-}$ (Figure 9). The low number of converted ECs reflects the low expression of *MCreM* from the *Cdh5-IRES-MCreM* locus. The mosaicism of the $Ctnnb1^{flex3/+}$ *Cdh5-IRES-MCreM* choroid plexus provides a nice internal control in the form of unrecombined ECs, and it demonstrates the cell autonomous nature of the conversion. We conclude from this experiment that differentiated capillary ECs in the choroid plexus possess a latent developmental plasticity that can be modulated by canonical WNT signaling.

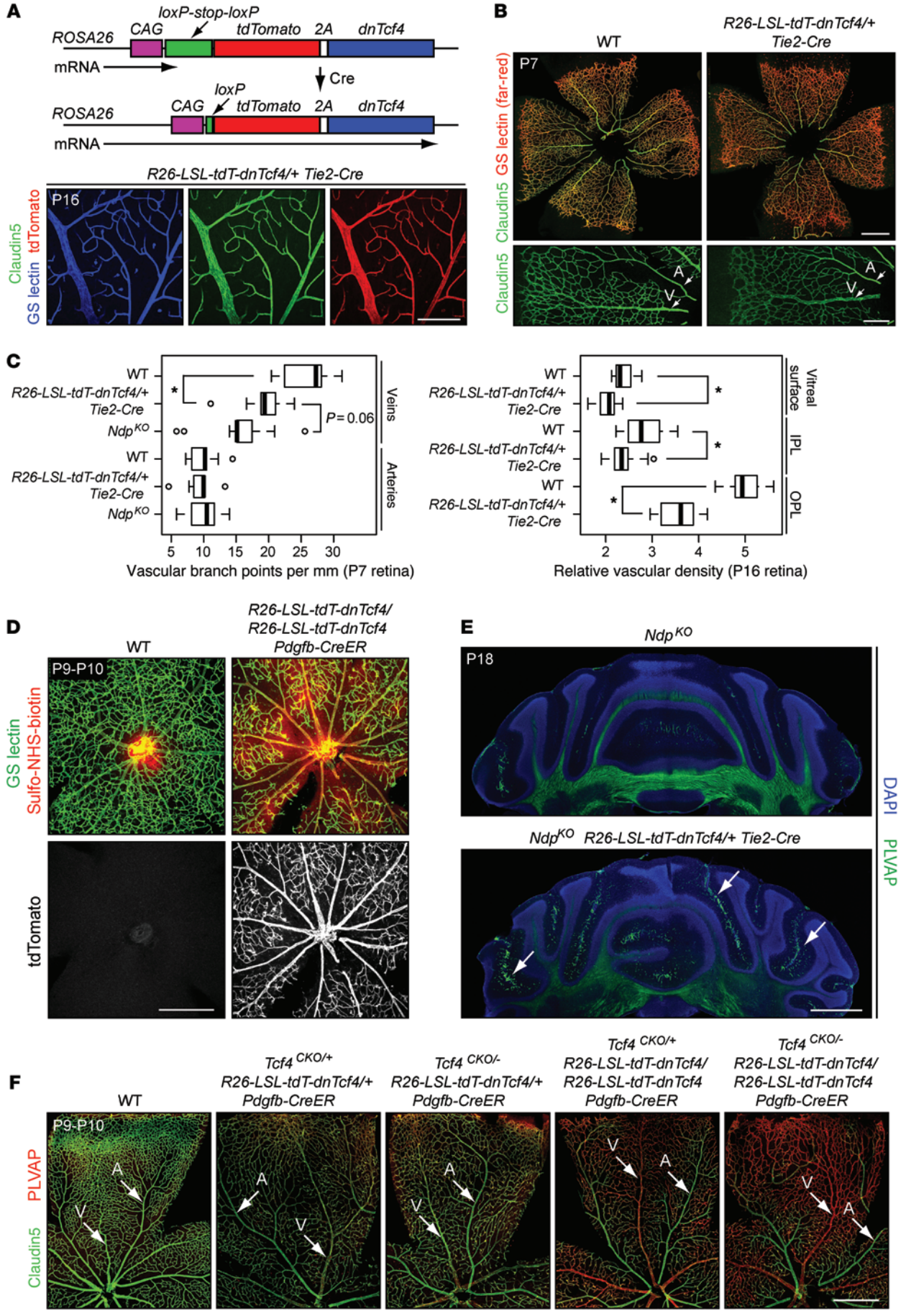
A
loxP-stop-loxP
CAG
tdTomato
2A
dnTcf4
ROSA26
mRNA
Cre
loxP
R26-LSL-tdT-dnTcf4/+ Tie2-Cre
P16
Claudin5
GS lectin
tdTomato
B
WT
R26-LSL-tdT-dnTcf4/+ Tie2-Cre
P7
GS lectin (far-red)
Claudin5
A
V
C
WT
R26-LSL-tdT-dnTcf4/+ Tie2-Cre
Ndp^KO
Veins
Arteries
P= 0.06
Vascular branch points per mm (P7 retina)
Vitreal surface
IPL
OPL
Relative vascular density (P16 retina)
D
WT
R26-LSL-tdT-dnTcf4/ R26-LSL-tdT-dnTcf4 Pdgfb-CreER
P9-P10
GS lectin
Sulfo-NHS-biotin
tdTomato
E
Ndp^KO
P18
DAPI
PLVAP
Ndp^KO R26-LSL-tdT-dnTcf4/+ Tie2-Cre
F
WT
Tcf4 CKO/+ R26-LSL-tdT-dnTcf4/+ Pdgfb-CreER
Tcf4 CKO/- R26-LSL-tdT-dnTcf4/+ Pdgfb-CreER
Tcf4 CKO/+ R26-LSL-tdT-dnTcf4/ R26-LSL-tdT-dnTcf4 Pdgfb-CreER
Tcf4 CKO/- R26-LSL-tdT-dnTcf4/ R26-LSL-tdT-dnTcf4 Pdgfb-CreER
P9-P10
PLVAP
Claudin5
A
V

Figure 11. Production of dnTCF4 in ECs mimics the phenotypes seen with loss of canonical WNT signaling in the retina and cerebellum. (**A**) The *R26-LSL-tdT-dnTcf4* knockin before and after Cre-mediated recombination (upper panel). EC accumulation of tdTomato in *R26-LSL-tdT-dnTcf4 Tie2-Cre* retina flat mounts (lower panel). Scale bar: 200 μm. (**B**) P7 *R26-LSL-tdT-dnTcf4/+ Tie2-Cre* retinas show a modest decrease in Claudin5 expression in veins and capillaries compared with WT controls. Scale bar: 500 μm (upper panels); 200 μm (lower panels). (**C**) Quantification of branch points from retinal veins and arteries at P7 (left panel) and vascular density in the 3 retinal layers at P16 (right panel). $^*P < 0.01$. (**D**) *R26-LSL-tdT-dnTcf4/R26-LSL-tdT-dnTcf4 Pdgfb-CreER* retinas (i.e., 2 alleles expressing *dnTcf4*) from P9–P10 mice treated with 50 μg 4HT at P3 show sulfo-NHS-biotin leakage and reduced vessel density (top panels). *Pdgfb-CreER* mediates nearly complete recombination at *R26* as assessed by tdTomato fluorescence (bottom panels). Scale bar: 400 μm. (**E**) Genetic interaction between *Ndp* and *R26-LSL-tdT-dnTcf4* with EC expression of *dnTcf4*. At P18, PLVAP$^+$ ECs increase in the vasculature of the Ndp^{KO}*;R26-LSL-tdT-dnTcf4/+ Tie2-Cre* cerebellum (lower panel; white arrows) compared with the Ndp^{KO} cerebellum (upper panel). Scale bar: 1 mm. (**F**) Synergistic effect of reducing or eliminating *Tcf4* and expressing different levels of *dnTcf4* in ECs. Flat-mount P9–P10 retinas from mice that had received 40 μg 4HT at P1. With each reduction in *Tcf4* or increase in *dnTcf4*, there are greater PLVAP expression and lower Claudin5 expression in veins and capillaries. Scale bar: 500 μm.

Transcriptional regulation is the major mechanism by which β-catenin influences CNS vascular growth and barrier function. As noted in the second paragraph of Results, β-catenin has 2 distinct functions: it regulates transcription by associating with TCF/LEF factors and it maintains the integrity of junctional complexes by associating with the cytosolic domain of E-cadherin (46). In principal, the decrease in β-catenin destruction induced by canonical WNT signaling could affect either or both of these functions. To extend the analysis of transcriptional versus junctional roles of β-catenin beyond embryonic vascular development (Figure 1, B–D), we analyzed the structure of the postnatal vasculature when $Ctnnb1^{dm}$ was the only functional *Ctnnb1* allele in vascular ECs.

In $Ctnnb1^{CKO/dm}$ *Pdgfb-CreER* mice treated with 4HT at P6 and examined at P10, the BBB was severely compromised, as determined by sulfo-NHS-biotin leakage, and there was widespread conversion of brain ECs from a PLVAP$^-$Claudin5$^+$ to a PLVAP$^+$Claudin5$^-$ state (Figure 10, A and B). In retinas of $Ctnnb1^{CKO/dm}$ *Pdgfb-CreER* mice treated with 4HT at P6 and examined at P10, development of the deep vascular plexus (between the inner and outer nuclear layers) was greatly reduced, capillary and vein ECs were converted to a PLVAP$^+$Claudin5$^-$ state, and the BRB was diffusely compromised, as observed in flat mount (Figure 10, C and D) and cross section (Figures 10E and Supplemental Figure 7). We note that the severity of the $Ctnnb1^{CKO/dm}$ *Pdgfb-CreER* retinal vascular phenotype cannot be directly compared with the phenotypes associated with constitutive loss of FZ4 or Ndp because the $Ctnnb1^{CKO/dm}$ *Pdgfb-CreER* phenotype reflects only a 4-day window of gene loss (4HT at P6 and sacrifice at P10). However, the milder CNS vascular phenotype seen in the constitutively recombined E11.5 $Ctnnb1^{CKO/dm}$ *Tie2-Cre* embryos compared with $Ctnnb1^{CKO/CKO}$ *Tie2-Cre* embryos (Figure 1, B–D) suggests either that the $Ctnnb1^{dm}$ allele is not completely defective in transcriptional regulation or that other β-catenin functions — such as β-catenin/E-cadherin complex formation — play a minor role in vascular development.

As a second experimental approach to assessing the role of β-catenin and TCF/LEF transcriptional regulation in CNS vascular development and barrier integrity, we constructed a Cre-activated knockin allele at the *ROSA26* locus that codes for a tdTomato reporter and a dominant negative (dn)TCF4 (also called TCF7L2; Figure 11A). dnTCF4 binds to its DNA targets, but lacks the β-catenin–binding domain and therefore fails to activate transcription (47); a similar derivative has been constructed for TCF3 (48). Its design was inspired by the discovery of a naturally occurring N-terminally truncated TCF4 isoform that functions as an antagonist of canonical WNT signaling. Experiments using several different cell types indicate that chromatin-bound β-catenin colocalizes with TCF4 (49, 50). EC-specific activation of 1 copy of *dnTcf4* produces a reduction in the density of the retinal vasculature in all 3 layers at P16, a difference that was presaged by a reduction in the number of venous branch points and a modest reduction in Claudin5 expression at P7 (Figure 11, B and C). EC-specific activation of 2 copies of *dnTcf4* produced a greater reduction in retinal vascular density and widespread BRB incompetence in the P9 retina (Figure 11D). Interestingly, at 3 months of age, retinas with this genotype showed PLVAP accumulation in veins but not in capillaries (Supplemental Figure 8B). This effect could not be attributed to differential production of dnTCF4 in the different types of blood vessels because visual inspection and quantitative analysis of pixel intensity revealed similar levels of accumulation of the cotranslated tdTomato reporter in capillaries and veins (Supplemental Figure 8B). In the cerebellum, activating 1 copy of *dnTcf4* in ECs had no effect on its own, but in combination with Ndp^{KO}, it increased the number of PLVAP$^+$ ECs above that observed in the Ndp^{KO} cerebellum (arrows in Figure 11E). In the postnatal brain with 2 copies of *dnTcf4*, a low density of PLVAP$^+$ ECs was found in multiple regions (data not shown).

To further explore the role of TCF4, we examined the retinal vasculature in mice with mutations in the *Tcf4* gene. Surprisingly, $Tcf4^{CKO/-}$ *Tie2-Cre* mice showed no anatomic retinal vascular defects and no BBB defects, as judged by sulfo-NHS-biotin perfusion. However, combining a reduction in *Tcf4* with expression of *dnTcf4* synergized to produce a change in PLVAP and Claudin5 expression, as might be expected if both proteins compete for the same DNA target sites. Specifically, with each additional allele producing dnTCF4 in ECs and with each reduction in the number of endogenous *Tcf4* alleles in ECs, there was a progressive increase in PLVAP and a progressive reduction in Claudin5 in retinal vein and capillary ECs at P9–P10 (Figure 11F). Similar to the effects seen with expressing *dnTcf4* on a WT background, in older retinas (P30) with various combinations of *dnTcf4* and *Tcf4* mutations, ECs with increased PLVAP and reduced Claudin5 were confined to vein ECs (Supplemental Figure 8A). These experiments implicate TCF4 as one of the LEF/TCF family members that mediate canonical WNT signaling in ECs, but the relatively modest effect that homozygous EC-specific loss of TCF4 had on vascular architecture implies that other family members are also active in these cells. These experiments also reveal a difference between vein and capillary ECs in their responses to perturbations in TCF4 function.

Taken together, the experiments with $Ctnnb1^{dm}$ and *dnTcf4* confirm and extend earlier observations (5, 6, 51), and they imply that β-catenin– and TCF/LEF-dependent transcriptional activa-

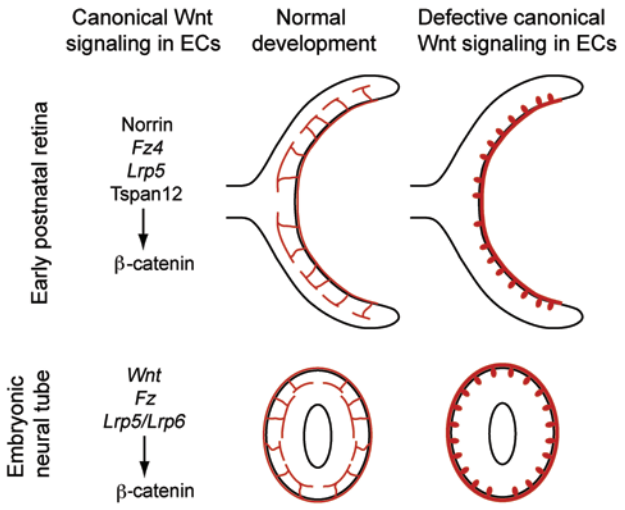

Figure 12. Schematic of angiogenesis defects in the neural tube and retina. Top, early postnatal retina showing vascular invasion in WT versus a canonical WNT-signaling–deficient mutant (loss of *Ndp* or *Fz4*). Bottom, E11.5 neural tube showing vascular invasion in WT versus a canonical WNT-signaling–deficient mutant (loss of *Ctnnb1* or *Lrp5* and *Lrp6*). In the mutant cases, there is stunted invasion with the formation of glomeruloid bodies and hypertrophy of the surface vasculature. On the left, the currently defined components that mediate canonical WNT signaling are shown for retinal and neural tube angiogenesis.

tion is the major mechanism by which canonical WNT signaling modulates retinal and brain vascular development and barrier formation and maintenance, but they leave open the possibility than nontranscriptional mechanisms may play a minor role.

Discussion

In this paper, we describe the responses of different subsets of developing and mature ECs to changes in the abundance of canonical WNT signaling components. These experiments reveal previously unappreciated region-specific and EC cell type–specific differences in sensitivity to perturbations in canonical WNT signaling. We also present evidence that Norrin/FZ4 signaling in the retina and cerebellum occurs predominantly or exclusively via activation of canonical WNT signaling (β-catenin stabilization) and that β-catenin mediates most of its effects on vascular development and BBB homeostasis via transcriptional regulation.

Diversity within the brain vasculature: canonical WNT signaling thresholds and the topography of BBB homeostasis. Beyond the universal division of all ECs into arterial, vein, and capillary subtypes, ECs that populate the bulk of the CNS vasculature have generally been viewed as a phenotypically uniform population. The exceptions to this generalization are the ECs in the vasculature of the posterior pituitary, the circumventricular organs, and the choroid plexus — specialized regions of the brain with highly permeable vessels (52). Our experiments indicate that there is another layer of phenotypic diversity among CNS ECs that can be revealed by compromising canonical WNT signaling. This diversity is especially striking in the cerebellum, where the BBB in the molecular layer is highly sensitive to a reduction in canonical WNT signaling and the BBB in the granule layer is largely resistant (e.g., Figure 2O, Figure 3H, and Figure 7B). These differences could reflect some combination of (a) intrinsic differences in sensitivity to canonical WNT signaling, (b) differences in the abundance or activity of Frizzled and LRP receptors in ECs, (c) differences in the local abundance or composition of canonical WNT ligands (WNTs and Norrin) and extracellular modulators of canonical WNT signaling (Dkk, Sost, and other binding proteins; ref. 53), and (d) regional variations in unrelated signal transduction pathways that could synergize with or antagonize canonical WNT signaling or that could otherwise compensate for a reduction in canonical WNT signaling. The data also imply that multiple regions of CNS vasculature have a level of canonical WNT signaling that is only marginally above the threshold for maintaining barrier integrity.

Canonical WNT signaling in EC development and homeostasis. The importance of WNT/FZ and Norrin/FZ signaling in CNS vascular development is now well established, but the striking similarities between embryonic neural tube and postnatal retinal vascularization defects produced by loss of canonical WNT signaling have not been widely appreciated. In both contexts, normal development involves a vascular plexus on the outer surface of the neuroepithelium that serves as a source of angiogenic ECs. In the absence of canonical WNT signaling, EC invasion is arrested near the neuroepithelial surface and the resulting clusters of ECs (glomeruloid bodies) do not produce a vascular plexus (Figure 12). The similarities between the neural tube and retinal vascularization phenotypes suggest that angiogenic ECs are using the same genetic regulatory circuits and cell biological programs in the 2 contexts. It would be interesting to extend this comparison by exploring the roles in neural tube vascularization of other signaling pathways such as Notch and Semaphorin/Plexin that have been studied in the context of retinal vascular development (54).

The roles of most of the genes that are regulated by canonical WNT signaling in ECs remain obscure. In the present experiments, 232 transcripts were observed to change more than 2-fold in WT retinas compared with Ndp^{KO} retinas, including 7 identified by Daneman et al. (42) as enriched in CNS over non-CNS vasculature. Earlier work identified and the present work confirms Sox17 as a transcription factor that is induced by Norrin/FZ4 signaling. Experiments in which constitutive production of Sox17 in $Fz4^{-/-}$ ECs in culture restored cell motility support a role for Sox17 in orchestrating the Norrin/FZ4 response (9). The diversity of EC transcripts that respond to Norrin/FZ4 signaling — including transporters, transcription factors, and enzymes — implies that canonical WNT signaling influences a wide variety of physiologic and cellular functions.

One of the most interesting features of canonical WNT signaling in ECs is its link to the plasticity of the barrier phenotype. In mature CNS ECs, activation or inhibition of canonical WNT signaling can induce or reverse the barrier state (present work; refs. 5, 10). It is interesting that after an experimentally induced reduction in canonical WNT signaling, the appearance of PLVAP is more rapid than the disappearance of Claudin5, a differential that could reflect the rapidity of transcriptional activation of PLVAP and a long half-life of Claudin5. This kinetic difference suggests that transient decrements in canonical WNT signaling might permit permeation of small molecules through capillary fenestrations without compromising EC-EC tight junctions.

Implications for diseases associated with BBB/BRB breakdown. Defects in Norrin/FZ4 signaling that lead to the most severe retinal hypovascularization phenotypes — Norrie disease (due to *NDP* mutation; ref. 15) and osteoporosis-pseudoglioma syndrome (due to homozygosity or compound heterozygosity for *LRP5* mutations; ref. 55) — are typically associated with little or no vision at birth. For these 2 disorders, postnatal interventions are unlikely to be efficacious. However, partial loss of Norrin/FZ4 signaling — as seen in FEVR caused by heterozygous loss of *FZD4*, *LRP5*, or *TSPAN12* — is associated with a wide range of disease severities, from subclinical to severe retinal traction and detachment (16–20, 56). The finding that $Fz4^{+/-}$ mice exhibit partial conversion of retinal ECs to a $PLVAP^{+}$ state suggests that the same EC conversion may be occurring in FEVR patients. If chronically reduced levels of Norrin/FZ signaling are causally related to FEVR pathogenesis, then a therapy that modestly enhances Norrin/FZ4 signaling in the retinal vasculature might block or slow disease progression.

Among FEVR patients whose DNA has been subjected to exome sequencing, approximately half have been found to harbor mutations in *TSPAN12*, *FZD4*, *NDP*, or *LRP5* (17). Recently, Collin et al. (57) identified mutations in the gene encoding the Zinc finger transcription factor *ZNF408* in 2 FEVR families, raising the number of FEVR genes to 5. The possibility that interactions among more than one disease or risk alleles may account for some of the clinical heterogeneity observed among FEVR patients who harbor the same allele was raised by Poulter et al. (20) based on their identification of homozygous *TSPAN12* mutations in several patients with severe FEVR symptoms. Kondo et al. (58) have made a similar observation in a patient with severe FEVR symptoms who was homozygous for a *FZD4* mutation. Our observations of multiple gene-gene interactions and low thresholds for anatomic and biochemical defects support this idea.

BRB defects are present in a wide variety of ophthalmic disorders, and BBB defects are present in a wide variety of neurologic disorders. BRB incompetence produces macular edema, and in the context of diabetic retinopathy or age-related macular degeneration, this condition can be treated by intraocular injection of anti-VEGF antibodies or soluble receptors (59). If Norrin/FZ4 signaling plays a role in regulating vascular permeability in the context of macular edema, then greater efficacy might be obtained by a combination therapy that both antagonizes VEGF and enhances Norrin/FZ4 signaling. In the brain, BBB breakdown accompanied by brain edema occurs in the context of inflammation and tissue injury, including trauma and stroke (60). It would be of great interest to determine whether this breakdown involves a decline in canonical WNT signaling in ECs.

BBB permeabilization for drug delivery. Promoting a transient disruption in the BBB for the purpose of enhancing CNS drug delivery has been an area of active investigation, but it has had limited success in the clinic. Early work focused on perfusing a hyperosmolar mannitol solution into the carotid artery to transiently shrink ECs and disrupt EC-EC junctions (61). Recent preclinical studies have shown promising results with intravascular microbubbles that absorb focused ultrasound energy to locally disrupt the BBB (62).

Using a function-blocking anti-FZ4 monoclonal antibody, Paes et al. (63) have demonstrated disruption of the BRB following systemic mAb delivery in adult mice. Extrapolating from the experiments of Paes et al. and from the genetic studies of WNT signaling in the adult CNS vasculature, it would be interesting to test whether transient pharmacologic inhibition of canonical WNT signaling could disrupt the BBB in a controlled fashion. The rapid induction of PLVAP in mouse ECs following loss of canonical WNT signaling suggests that a brief treatment with canonical pathway inhibitors might transiently induce EC fenestrations without significantly perturbing EC-EC junctions. Treatment for a longer duration would be predicted to eventually weaken or disrupt EC-EC junctions. Both short- and long-term pharmacologic blockade of WNT signaling might usefully enhance drug delivery to the CNS. We also note that pharmacologic and ultrasound/micro-bubble approaches might be synergistic. For example, if WNT signaling in CNS ECs could be transiently inhibited, the reduction in EC-EC junction stability might render the vasculature more sensitive to focused ultrasound/microbubble stress, with reduced risk for tissue injury.

Methods

Mice. The following transgenic mouse alleles were used: $Ctnnb1^{dm}$ (25), $Ctnnb1^{flex3}$ (41), $Lrp5^{-}$ (21), $Lrp6^{CKO}$ (23), *BAT-gal* (40), $Tcf4^{CKO}$ (64), *Tie2-Cre* (24), *Pdgfb-CreER* (26), $Fz4^{-}$ (65), $Fz4^{CKO}$ (9), and Ndp^{KO} (9). The *R26-LSL-tdT-dnTcf4* allele was generated by inserting a cytomegalovirus/β-actin promoter/enhancer (CAG) membrane tethered tdTomato (i.e., tdTomato tagged with an N-terminal myristoylation site)-triple-myc-2A-dnTcf4 cassette at the *ROSA26* locus by homologous recombination in ES cells; see Tang et al. (66) for a description of the 2A peptide technology. The dominant-negative TCF4 polypeptide consists of a methionine followed by amino acids 162–460 of TCF4 (TCF7L2) transcript variant 1 (47). The *Cdh5-IRES-MCreM* allele was constructed by inserting an *IRES-Mer-Cre-Mer* cassette (44) into the 3′ UTR of the *Cdh5* gene by homologous recombination in ES cells. ES cells with the correct targeting event were identified by Southern blotting and injected into blastocysts. The resulting chimeric founders were bred using standard methods.

Antibodies and other reagents. Antibodies used in this study were as follows: rabbit anti-calbindin (Swant; CB38a); rat anti-mouse CD102/ICAM2 (BD Biosciences; 553326); rabbit anti–GLUT-1 (Thermo Scientific; RB-9052-P0), mouse anti–Claudin5 clone 4C3C2, Alexa Fluor 488 conjugate (Invitrogen; 352588); rat anti-PLVAP/MECA-32 (BD Biosciences — Pharmingen; 553849); mouse anti–α smooth muscle actin clone 1A4, Cy3 conjugate (Sigma-Aldrich; C6198), rabbit anti–Pdgfr-β mAb (Cell Signaling; 3169), chicken anti–β-galactosidase (Abcam; 9361-250), and rabbit anti–cleaved caspase 3 (Cell Signaling; 9661). Alex Fluor–labeled secondary antibodies and GS lectin (Isolectin; GS-IB4) were from Invitrogen, Texas red streptavidin was from Vector Labs (SA5006), and 488 nm streptavidin was from Invitrogen (S11223).

Preparation and administration of 4HT. Solid 4HT (Sigma-Aldrich) was dissolved in ethanol at 20 mg/ml, and then 4 volumes of sunflower seed oil (Sigma-Aldrich) was added; the sample was extensively vortexed (>1 hour) at room temperature and stored in aliquots at –80°C. The thawed samples were vortexed and diluted as needed in sunflower seed oil prior to i.p. injection of 50 to 100 μl.

Histochemistry and immunohistochemistry. For retinal vasculature, mouse eyes were fixed in 1% paraformaldehyde (PFA) in PBS at 4°C for 4 to 6 hours prior to dissection. Whole-mount retinas were incubated at 4°C overnight in primary antibodies diluted in PBSTC

(PBS plus 0.5% Triton X-100 plus 0.1 mM $CaCl_2$) plus 10% normal goat serum, washed in PBSTC for 6 to 8 hours, and incubated at 4°C overnight in secondary antibodies diluted in PBSTC plus 10% normal goat serum. The retinas were washed in PBSTC and flat mounted in Fluoromount G (EM Sciences; 17984-25). For brain vasculature, deeply anesthetized mice were perfused with PBS followed by 1% PFA in PBS. Dissected brains were immersed in cold 100% methanol at 4°C overnight and then rehydrated in PBS for 2 to 4 hours at 4°C. Brains were dissected and embedded in 3% agarose and 100- to 150-μm sections were cut on a vibratome, immunostained, and imaged. For immunostaining with rat mAbs, 0.25% to 1% mouse serum was used as a competitive blocker during incubation with the secondary antibody to lower anti-mouse crossreactivity. Whole-mount E11.5 embryos were immunostained, dehydrated, and clarified in benzyl benzoate: benzyl alcohol as described in Hua et al. (67). Images were captured using a Zeiss LSM700 confocal microscope and processed with Zen, Adobe Photoshop, ImageJ (http://imagej.nih.gov/ij/), and Adobe Illustrator software.

Arteries and veins are readily distinguished in retinal flat mounts. When compared at the same radial distance from the optic disc, arteries have a smaller diameter and are surrounded by a capillary-free zone. This assignment is confirmed by immunostaining for smooth muscle actin, which is present in perivascular cells that surround arteries but not in pericytes around veins or capillaries.

Evans blue and sulfo-NHS-biotin injections. For sulfo-NHS-biotin perfusion, deeply anesthetized mice were perfused with 10- to 30-ml 0.3 mg/ml sulfo-NHS-LC-Biotin (Thermo Scientific; 21335) in PBS, followed by 2% PFA in PBS. Eyes were postfixed in 1% PFA at 4°C for 4 to 6 hours prior to retina dissection. Whole-mount retinas and 100- to 150-μm vibratome sections of brain were incubated in Texas red streptavidin (Vector; SA-5006) diluted in PBSTC with 10% normal goat serum, washed in PBSTC, and mounted in Fluoromount G. For Evans blue leakage, 100 μl of 2% Evans blue (Sigma-Aldrich; E-2129) was injected i.p. 24 hours prior to perfusion with 4% PFA in PBS. Brains were dissected and photographed intact.

Whole-retina RNAseq. Three batches of total RNA were extracted using TRIzol (Invitrogen) and the RNeasy kit (QIAGEN). Each batch was prepared from 4 to 8 P10 retinas (2–4 mice) per genotype: WT, Ndp^{KO}, $Ctnnb1^{flex3/+}$ *PdgfbcreER*, and Ndp^{KO} $Ctnnb1^{flex3/+}$ *PdgfbcreER*. By analyzing whole retinas rather than purified ECs, we have presumably eliminated the possibility of artifactual transcriptome changes associated with postmortem cell manipulation. All mice received 20 μg 4HT i.p. at P3, thus avoiding the possibility that differential transcript abundances might be referable to differences in 4HT exposure. The 3 batches of RNA were pooled for RNAseq library construction using the TruSeq RNA Sample Prep Kit v2 (Illumina). From 27 to 65 million 50 base single–end reads were obtained from each of the 4 bar-coded libraries using an Illumina HiSeq2000. Raw reads were mapped to the reference genome (mm10) using TopHat, and the relative abundance of each transcript was calculated with Cuffdiff. The sets of transcripts enriched in brain ECs relative to peripheral ECs or enriched in brain ECs relative to neurons and glia were derived from the analyses of Daneman et al. (42). Transcripts with FPKM greater than 0.3 for any of the samples used in a particular comparison were included. Y chromosome transcripts were excluded from the analysis to avoid variations related to gender. The RNAseq data has been deposited in the GEO database (GSE56461).

Quantification of vascular branching points. Starting with images of retina flat mounts, retinal vascular branch points were counted along each radial vein or artery starting at the optic disc and terminating at a point that was 0.75 of the radial distance from the optic disc to the edge of the vascular plexus. The number of branch points was then normalized to the total length of the vessel.

Quantification of retinal vascular coverage. For the $Ctnnb1^{flex3}$ and the *dnTcf4* experiments, 4 Z-stacked images of retina flat mounts, each covering 0.64 × 0.64 mm^2 and offset approximately 0.3 to 0.6 mm from the optic disc, were captured from each GS lectin–stained retina using a Zeiss LSM700 microscope. For each of the 3 vascular beds (at the vitreal surface, IPL, and OPL), the images were thresholded, binarized, and skeletonized using ImageJ. The relative vascular lengths were measured by computing the pixel coverage (which is proportional to length) of the skeletonized vessels.

Quantification of cerebellar granule cell death. Apoptotic cells were detected in 150-μm floating sections of cerebellum by immunostaining for anti-cleaved caspase 3. One section (from a matched cerebellar location) was counted per mouse, and 3, 6, and 8 WT, $Fz4^{-/-}$, and $Fz4^{-/-}$ $Ctnnb1^{flex3/+}$ *Pdgfb-Cre* mice, respectively, were analyzed.

Quantification of β-galactosidase positive retinal and cerebellar ECs. β-Galactosidase$^+$ ECs were detected in whole retinas and in 150-μm floating sections of cerebellum by immunostaining with anti–β-galactosidase combined with GS lectin binding. For the retina, all β-galactosidase$^+$ ECs were counted from flat-mount images. For the cerebellum, Z-stacked images encompassing approximately 15 μm were collapsed and the β-galactosidase$^+$ ECs in the vasculature along the surface of the molecular layer were counted.

Semiquantitative scoring of BBB breakdown. Confocal images of 100- to 150-μm vibratome sections from mice perfused with sulfo-NHS-biotin and stained with Texas red streptavidin were scored by 2 observers (Y. Wang and J. Nathans) using 4 categories for BBB breakdown: absent (i.e., indistinguishable from WT), mild, moderate, or severe. Examples of mild, moderate, and severe breakdown of the BBB in the cerebellum are seen in Figure 3, G–I, respectively.

OKR. OKR recordings and analysis were performed on head-fixed mice using infrared video recordings of pupil position as described in Cahill and Nathans (68). The visual stimulus was projected onto the inner walls of a vertical cylinder surrounding the head-posted mouse, and during alternating 30-second intervals, the stimulus consisted either of horizontally rotating vertical black and white stripes or a uniform gray of equivalent mean intensity, represented, respectively, by stripes and by gray zones at the top of Figure 8H.

Statistical analysis and graphical presentations. Box and whisker plots (RStudio) show, at their centers, the median (horizontal bar) and the 25th and 75th percentiles (box). The whiskers are located at the positions of the furthest-flung data points above or below the mean that are within a distance of 1.5 times the 25th–75th percentile distance (i.e., height of the box) either below the 25th percentile position or above the 75th percentile position. Any data points beyond the whiskers are plotted individually. For statistical analysis, an unpaired 2-tailed Student's *t* test was performed, and $P < 0.01$ was considered significant.

Study approval. Mice were handled and housed according to the approved Institutional Animal Care and Use Committee (IACUC) protocol MO13M469 of the Johns Hopkins Medical Institutions. All animal studies were approved by the IACUC of the Johns Hopkins Medical Institutions.

Acknowledgments

The authors thank the following colleagues for sharing reagents: Melinda Angus-Hill (*Tcf4*^{CKO} mice), Konrad Basler (*Ctnnb1*^{dm} mice), Richard Behringer (*Ctnnb1*^{flex3} mice), Greg Lemke (*dnTcf4* plasmid), Bart Williams (*Lrp6*^{CKO} mice), and Michael Reth (*Mer-CreMer* plasmid). Zheng Kuang provided invaluable input on the analysis of RNAseq data. The authors thank Hao Chang for comments on the manuscript. This work was supported by the Howard Hughes Medical Institute, the National Eye Institute (EY018637 to Jeremy Nathans), the Ellison Medical Research Foundation, and an NIH National Research Service Award granted by the National Eye Institute (F32EY0222274 to Max Tischfield).

Address correspondence to: Jeremy Nathans, 805 PCTB, 725 North Wolfe Street, Johns Hopkins University School of Medicine, Baltimore, Maryland 21205, USA. Phone: 410.955.4679; E-mail: jnathans@jhmi.edu.

Max Tischfield's present address is: Children's Hospital, Boston, Massachusetts, USA.

1. Aird WC. Phenotypic heterogeneity of the endothelium: I. structure, function, and mechanisms. *Circ Res*. 2007;100(2):158–173.
2. Aird WC. Phenotypic heterogeneity of the endothelium: II. representative vascular beds. *Circ Res*. 2007;100(2):174–190.
3. Ballermann BJ. Glomerular endothelial cell differentiation. *Kidney Int*. 2005;67(5):1668–1671.
4. Hawkins BT, Davis TP. The blood-brain barrier/neurovascular unit in health and disease. *Pharmacol Rev*. 2005;57(2):173–185.
5. Liebner S, et al. Wnt/β-catenin signaling controls development of the blood-brain barrier. *J Cell Biol*. 2008;183(3):409–417.
6. Stenman JM, Rajagopal J, Carroll TJ, Ishibashi M, McMahon J, McMahon AP. Canonical Wnt signaling regulates organ-specific assembly and differentiation of CNS vasculature. *Science*. 2008;322(5905):1247–1250.
7. Daneman R, Agalliu D, Zhou L, Kuhnert F, Kuo CJ, Barres BA. Wnt/β-catenin signaling is required for CNS, but not non-CNS, angiogenesis. *Proc Natl Acad Sci U S A*. 2009;106(2):641–646.
8. Xu Q, et al. Vascular development in the retina and inner ear: control by Norrin and Frizzled-4, a high-affinity ligand-receptor pair. *Cell*. 2004;116(6):883–895.
9. Ye X, et al. Norrin, Frizzled-4, and Lrp5 signaling in endothelial cells controls a genetic program for retinal vascularization. *Cell*. 2009;139(2):285–298.
10. Wang Y, Rattner A, Zhou Y, Williams J, Smallwood PM, Nathans J. Norrin/Frizzled4 signaling in retinal vascular development and blood brain barrier plasticity. *Cell*. 2012;151(6):1332–1344.
11. Rehm HL, et al. Vascular defects and sensorineural deafness in a mouse model of Norrie disease. *J Neurosci*. 2002;22(11):4286–4292.
12. Xia CH, et al. A model for familial exudative vitreoretinopathy caused by LPR5 mutations. *Hum Mol Genet*. 2008;17(11):1605–1612.
13. Junge HJ, et al. TSPAN12 regulates retinal vascular development by promoting Norrin- but not Wnt-induced FZD4/β-catenin signaling. *Cell*. 2009;139(2):299–311.
14. Ye X, Wang Y, Nathans J. The Norrin/Frizzled4 signaling pathway in retinal vascular development and disease. *Trends Mol Med*. 2010;16(9):417–425.
15. Berger W, Ropers H. Norrie disease. In: Scriver CR, Beaudet AL, Sly WS, Valle D, eds. *The Metabolic And Molecular Bases Of Inherited Disease*. New York, New York, USA: McGraw-Hill; 2001:5977–5985.
16. Qin M, Hayashi H, Oshima K, Tahira T, Hayashi K, Kondo H. Complexity of the genotype-phenotype correlation in familial exudative vitreoretinopathy with mutations in the LRP5 and/or FZD4 genes. *Hum Mutat*. 2005;26(2):104–112.
17. Nikopoulos K, et al. Next-generation sequencing of a 40 Mb linkage interval reveals TSPAN12 mutations in patients with familial exudative vitreoretinopathy. *Am J Hum Genet*. 2010;86(2):240–247.
18. Nikopoulos K, et al. Overview of the mutation spectrum in familial exudative vitreoretinopathy and Norrie disease with identification of 21 novel variants in FZD4, LRP5, and NDP. *Hum Mutat*. 2010;31(6):656–666.
19. Robitaille JM, et al. The role of Frizzled-4 mutations in familial exudative vitreoretinopathy and Coats disease. *Br J Ophthalmol*. 2011;95(4):574–579.
20. Poulter JA, et al. Recessive mutations in TSPAN12 cause retinal dysplasia and severe familial exudative vitreoretinopathy (FEVR). *Invest Ophthalmol Vis Sci*. 2012;53(6):2873–2879.
21. Kato M, et al. Cbfa1-independent decrease in osteoblast proliferation, osteopenia, and persistent embryonic eye vascularization in mice deficient in Lrp5, a Wnt coreceptor. *J Cell Biol*. 2002;157(2):303–314.
22. Pinson KI, Brennan J, Monkley S, Avery BJ, Skarnes WC. An LDL-receptor-related protein mediates Wnt signalling in mice. *Nature*. 2000;407(6803):535–538.
23. Joeng KS, Schumacher CA, Zylstra-Diegel CR, Long F, Williams BO. Lrp5 and Lrp6 redundantly control skeletal development in the mouse embryo. *Dev Biol*. 2011;359(2):222–229.
24. Kisanuki YY, Hammer RE, Miyazaki J, Williams SC, Richardson JA, Yanagisawa M. Tie2-Cre transgenic mice: a new model for endothelial cell-lineage analysis in vivo. *Dev Biol*. 2001;230(2):230–242.
25. Valenta T, et al. Probing transcription-specific outputs of β-catenin in vivo. *Genes Dev*. 2011;25(24):2631–2643.
26. Claxton S, Kostourou V, Jadeja S, Chambon P, Hodivala-Dilke K, Fruttiger M. Efficient, inducible Cre-recombinase activation in vascular endothelium. *Genesis*. 2008;46(2):74–80.
27. Stan RV, Kubitza M, Palade GE. PV-1 is a component of the fenestral and stomatal diaphragms in fenestrated endothelia. *Proc Natl Acad Sci U S A*. 1999;96(23):13203–13207.
28. Weinberg RA. *The Biology Of Cancer*. 2nd ed. New York, New York, USA: Garland Science; 2014.
29. Ye X, Wang Y, Rattner A, Nathans J. Genetic mosaic analysis reveals a major role for Frizzled 4 and Frizzled 8 in controlling ureteric growth in the developing kidney. *Development*. 2011;138(6):1161–1172.
30. Ye X, Smallwood P, Nathans J. Expression of the Norrie disease gene (Ndp) in developing and adult mouse eye, ear, and brain. *Gene Expr Patterns*. 2011;11(1–2):151–155.
31. Chen J, et al. Retinal expression of Wnt-pathway mediated genes in low-density lipoprotein receptor-related protein 5 (Lrp5) knockout mice. *PLoS One*. 2012;7(1):e30203.
32. Wu H, et al. Cellular resolution maps of X chromosome inactivation: implications for neural development, function, and disease. *Neuron*. 2014;81(1):103–119.
33. Reese BE, Tan SS. Clonal boundary analysis in the developing retina using X-inactivation transgenic mosaic mice. *Semin Cell Dev Biol*. 1998;9(3):285–292.
34. Janda CY, Waghray D, Levin AM, Thomas C, Garcia KC. Structural basis of Wnt recognition by Frizzled. *Science*. 2012;337(6090):59–64.
35. Ke J, et al. Structure and function of Norrin in assembly and activation of a Frizzled 4-Lrp5/6 complex. *Genes Dev*. 2013;27(21):2305–2319.
36. Kohn AD, Moon RT. Wnt and calcium signaling: β-catenin-independent pathways. *Cell Calcium*. 2005;38(3–4):439–446.
37. Goodrich LV, Strutt D. Principles of planar polarity in animal development. *Development*. 2011;138(10):1877–1892.
38. Descamps B, et al. Frizzled 4 regulates arterial network organization through noncanonical Wnt/planar cell polarity signaling. *Circ Res*. 2012;110(1):47–58.
39. Deng C, Reddy P, Cheng Y, Luo CW, Hsiao CL, Hsueh AJ. Multi-functional Norrin is a ligand for the LGR4 receptor. *J Cell Sci*. 2013;126(pt 9):2060–2068.
40. Maretto S, et al. Mapping Wnt/β-catenin signaling during mouse development and in colorectal tumors. *Proc Natl Acad Sci U S A*. 2003;100(6):3299–3304.
41. Harada N, et al. Intestinal polyposis in mice with a dominant stable mutation of the β-catenin gene. *EMBO J*. 1999;18(21):5931–5942.
42. Daneman R, Zhou L, Agalliu D, Cahoy JD, Kaushal A, Barres BA. The mouse blood-brain barrier transcriptome: a new resource for understanding the development and function of brain endothelial cells. *PLoS One*. 2010;5(10):e13741.
43. Corada M, et al. Sox17 is indispensable for acquisition and maintenance of arterial identity. *Nat Commun*. 2013;4:2609.

44. Verrou C, Zhang Y, Zürn C, Schamel WW, Reth M. Comparison of the tamoxifen regulated chimeric Cre recombinases MerCreMer and CreMer. *Biol Chem*. 1999;380(12):1435–1438.
45. Sturrock RR. A morphological study of the development of the mouse choroid plexus. *J Anat*. 1979;129(4):777–793.
46. Valenta T, Hausmann G, Basler K. The many faces and functions of β-catenin. *EMBO J*. 2012;31(12):2714–2736.
47. Vacik T, Stubbs JL, Lemke G. A novel mechanism for the transcriptional regulation of Wnt signaling in development. *Genes Dev*. 2011;25(17):1783–1795.
48. Wu CI, et al. Function of Wnt/β-catenin in counteracting Tcf3 repression through the Tcf3-β-catenin interaction. *Development*. 2012;139(12):2118–2129.
49. Bottomly D, Kyler SL, McWeeney SK, Yochum GS. Identification of β-catenin binding regions in colon cancer cells using ChIP-Seq. *Nucleic Acids Res*. 2010;38(17):5735–5745.
50. Schuijers J, Mokry M, Hatzis P, Cuppen E, Clevers H. Wnt-induced transcriptional activation is exclusively mediated by TCF/LEF. *EMBO J*. 2014;33(2):146–156.
51. Cattelino A, et al. The conditional inactivation of the β-catenin gene in endothelial cells causes a defective vascular pattern and increased vascular fragility. *J Cell Biol*. 2003;162(6):1111–1122.
52. Sisó S, Jeffrey M, González L. Sensory circumventricular organs in health and disease. *Acta Neuropathol*. 2010;120(6):689–705.
53. Cruciat CM, Niehrs C. Secreted and transmembrane Wnt inhibitors and activators. *Cold Spring Harb Perspect Biol*. 2013;5(3):a015081.
54. Potente M, Gerhardt H, Carmeliet P. Basic and therapeutic aspects of angiogenesis. *Cell*. 2011;146(6):873-887.
55. Gong Y, et al. LDL receptor-related protein 5 (LRP5) affects bone accrual and eye development. *Cell*. 2001;107(4):513-523.
56. Ranchod TM, Ho LY, Drenser KA, Capone A Jr, Trese MT. Clinical presentation of familial exudative vitreoretinopathy. *Ophthalmology*. 2011;118(10):2070–2075.
57. Collin RW, et al. ZNF408 is mutated in familial exudative vitreoretinopathy and is crucial for the development of zebrafish retinal vasculature. *Proc Natl Acad Sci U S A*. 2013;110(24):9856–9861.
58. Kondo H, Qin M, Tahira T, Uchio E, Hayashi K. (2007) Severe form of familial exudative vitreoretinopathy caused by homozygous R417Q mutation in frizzled-4 gene. *Ophthalmic Genet*. 2007; 28(4):220–223.
59. Chong V. Biological, preclinical and clinical characteristics of inhibitors of vascular endothelial growth factors. *Ophthalmologica*. 2012;227(suppl 1):2–10.
60. Obermeier B, Daneman R, Ransohoff RM. Development, maintenance and disruption of the blood-brain barrier. *Nat Med*. 2013;19(12):1584–1596.
61. Neuwelt EA, Diehl JT, Vu LH, Hill SA, Michael AJ, Frenkel EP. Monitoring of methotrexate delivery in patients with malignant brain tumors after osmotic blood-brain barrier disruption. *Ann Intern Med*. 1981;94(4 pt 1):449–454.
62. Aryal M, Arvanitis CD, Alexander PM, McDannold N. Ultrasound-mediated blood-brain barrier disruption for targeted drug delivery in the central nervous system. *Adv Drug Deliv Rev*. 2014;72C:94–109.
63. Paes KT, et al. Frizzled 4 is required for retinal angiogenesis and maintenance of the blood-retina barrier. *Invest Ophthalmol Vis Sci*. 2011;52(9):6452–6461.
64. Angus-Hill ML, Elbert KM, Hidalgo J, Capecchi MR. T-cell factor 4 functions as a tumor suppressor whose disruption modulates colon cell proliferation and tumorigenesis. *Proc Natl Acad Sci U S A*. 2011;108(12):4914-4919.
65. Wang Y, Huso D, Cahill H, Ryugo D, Nathans J. Progressive cerebellar, auditory, and esophageal dysfunction caused by targeted disruption of the Frizzled-4 gene. *J Neurosci*. 2001;21(13):4761–4771.
66. Tang W, et al. Faithful expression of multiple proteins via 2A-peptide self-processing: a versatile and reliable method for manipulating brain circuits. *J Neurosci*. 2009;29(27):8621–8629.
67. Hua ZL, Smallwood PM, Nathans J. Frizzled3 controls axonal development in distinct populations of cranial and spinal motor neurons. *Elife*. 2013;2:e01482.
68. Cahill H, Nathans J. The optokinetic reflex as a tool for quantitative analyses of nervous system function in mice: application to genetic and drug-induced variation. *PLoS One.* 2008;3(4):e2055.
69. Huang L, Rattner A, Liu H, Nathans J. How to draw the line in biomedical research. *Elife*. 2013;2:e00638.